iScience

CellPress
OPEN ACCESS

Article

CircPOLA2 sensitizes non-small cell lung cancer cells to ferroptosis and suppresses tumorigenesis via the Merlin-YAP signaling pathway

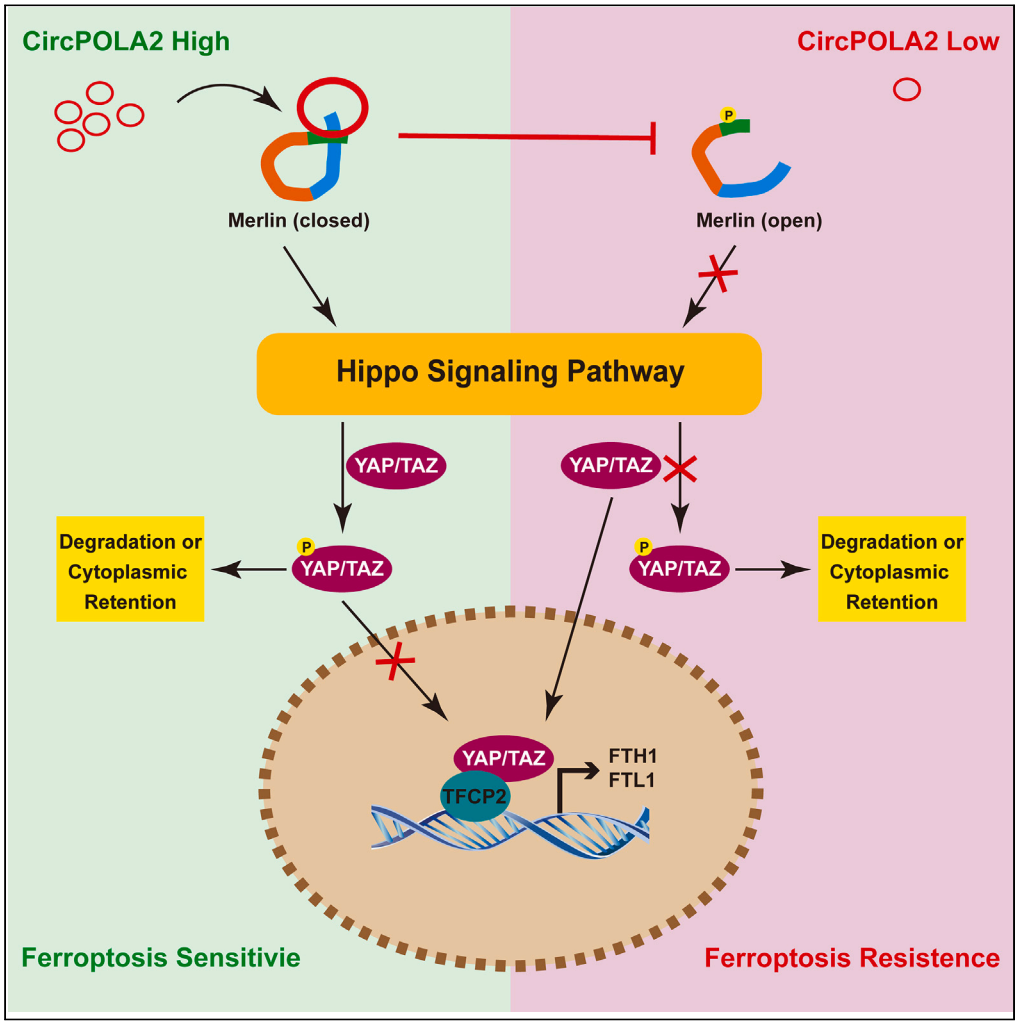

Kaiying Xu, Guangxia Wei, Wanghong Qi, ..., Shijiang Wang, Feng Yang, Jian Tang

feng_yang@ncu.edu.cn (F.Y.)
tangjianku@yeah.net (J.T.)

Highlights

CircPOLA2 is downregulated in NSCLC and negatively correlates with the clinical stage

CircPOLA2 sensitizes NSCLC cells to ferroptosis and inhibits tumorigenesis

CircPOLA2 activates the Hippo pathway by limiting the phosphorylation of Merlin (S518)

Targeting the circPOLA2-Merlin-YAP axis is a promising therapeutic strategy for NSCLC

Xu et al., iScience 27, 110832
September 20, 2024
https://doi.org/10.1016/j.isci.2024.110832

iScience

CellPress
OPEN ACCESS

Article

CircPOLA2 sensitizes non-small cell lung cancer cells to ferroptosis and suppresses tumorigenesis via the Merlin-YAP signaling pathway

Kaiying Xu,[1] Guangxia Wei,[1] Wanghong Qi,[1] Chunlin Ye,[1] Yangyang Liu,[2] Shijiang Wang,[3] Feng Yang,[3,*] and Jian Tang[1,4,5,*]

SUMMARY

Circular RNAs (circRNAs) have been implicated in the tumorigenesis of non-small cell lung cancer (NSCLC). Ferroptosis is considered a mechanism to suppress tumorigenesis. Herein, we identified a downregulated circRNA, circPOLA2 (hsa_circ_0004291), in NSCLC tissues and found that it was correlated with advanced clinical stage in patients. Nuclear-cytoplasmic fractionation assays and FISH assays confirmed that circPOLA2 was predominantly localized in the cytoplasm. Overexpression of circPOLA2 promoted lipid peroxidation and ferroptosis in NSCLC cells, thereby inhibiting cell proliferation and migration, while knockdown of circPOLA2 exerted the opposite effects. Mechanistically, circPOLA2 interacted with Merlin, a critical regulator of the Hippo pathway, and restricted Merlin phosphorylation at S518, leading to the activation of the Hippo pathway. In addition, circPOLA2 enhanced ferroptosis in NSCLC cells by activating the Hippo pathway. Together, circPOLA2 sensitizes cells to ferroptosis and suppresses tumorigenesis in NSCLC by facilitating Merlin-mediated activation of the Hippo signaling pathway.

INTRODUCTION

Lung cancer is the leading cause of cancer death worldwide, and non-small cell lung cancer (NSCLC) accounts for 80%–85% of lung cancer cases.[1,2] With advances in surgery, targeted therapy, and immunotherapy, the 5-year survival rate has reached 61% for patients with early-stage lung cancer; however, the overall 5-year survival rate is only 23% because many patients are diagnosed at an advanced stage.[3] Therefore, further research into the molecular mechanisms underlying NSCLC development and metastasis is urgently needed to develop novel diagnostic and therapeutic strategies.

Circular RNAs (circRNAs) are a class of covalently closed single-stranded RNA molecules that are mainly generated by back-splicing of pre-mRNAs.[4] Increasing evidence has shown that circRNAs are involved in almost all human malignancies, including NSCLC, through miRNA sponging, protein binding, or translation.[5] Dysregulated circRNAs have shown promising efficacy as biomarkers or therapeutic targets for lung cancer.[6] However, to date, no circRNA has been exploited for the clinical treatment of lung cancer, and most circRNAs have been found to act as miRNA sponges in the pathogenesis of lung cancer; thus, the other potential mechanisms underlying the role of circRNAs in tumor progression may have been ignored. Therefore, further efforts are needed to comprehensively elucidate the role of circRNAs in NSCLC.

Ferroptosis is a distinct form of regulated cell death (RCD) caused by the iron-dependent peroxidation of polyunsaturated fatty acid (PUFA)-containing PLs (PUFA-PLs) on the cell membrane, which is mainly mediated by the iron-catalyzed Fenton reaction.[7] To date, four cellular antioxidant systems have been found to act as ferroptosis defense mechanisms by directly neutralizing lipid peroxides, including the GPX4-GSH, FSP1-CoQH2, DHODH-CoQH2, and GCH1-BH4 systems.[8] Accumulating evidence indicates that ferroptosis is a natural tumor suppression mechanism, and several oncogenic signaling pathways and tumor suppressors have been shown to inhibit or promote ferroptosis respectively. For example, mTOR complex1[9] and mutant KRAS[10,11] promote tumorigenesis by inhibiting ferroptosis, whereas P53[12] and BAP1[13] exert tumor suppressor effects in part by promoting ferroptosis. Recently, several studies have reported that circRNAs increase the ferroptosis resistance of cancer cells by sponging miRNAs that target components of the ferroptosis defense system, such as circPVT1 in esophageal squamous cell carcinoma,[14] circGFRA1 in breast cancer,[15] circ_0067934[16] and circKIF4A[17] in thyroid cancer, and circDTL in NSCLC.[18] However, apart from acting as microRNA sponges, few studies have reported the other mechanisms mediating the regulatory effect of circRNAs on ferroptosis in cancer.[19]

[1]Department of Thoracic Surgery, The First Affiliated Hospital, Jiangxi Medical College, Nanchang University, Nanchang 330000, People's Republic of China
[2]Department of Oncology, The First Affiliated Hospital, Jiangxi Medical College, Nanchang University, Nanchang 330000, People's Republic of China
[3]Department of Orthopedic Surgery, The First Affiliated Hospital, Jiangxi Medical College, Nanchang University, Nanchang 330000, People's Republic of China
[4]National Regional Center for Respiratory Medicine, China Japan Friendship Jiangxi Hospital, Nanchang 330000, People's Republic of China
[5]Lead contact
*Correspondence: feng_yang@ncu.edu.cn (F.Y.), tangjianku@yeah.net (J.T.)
https://doi.org/10.1016/j.isci.2024.110832

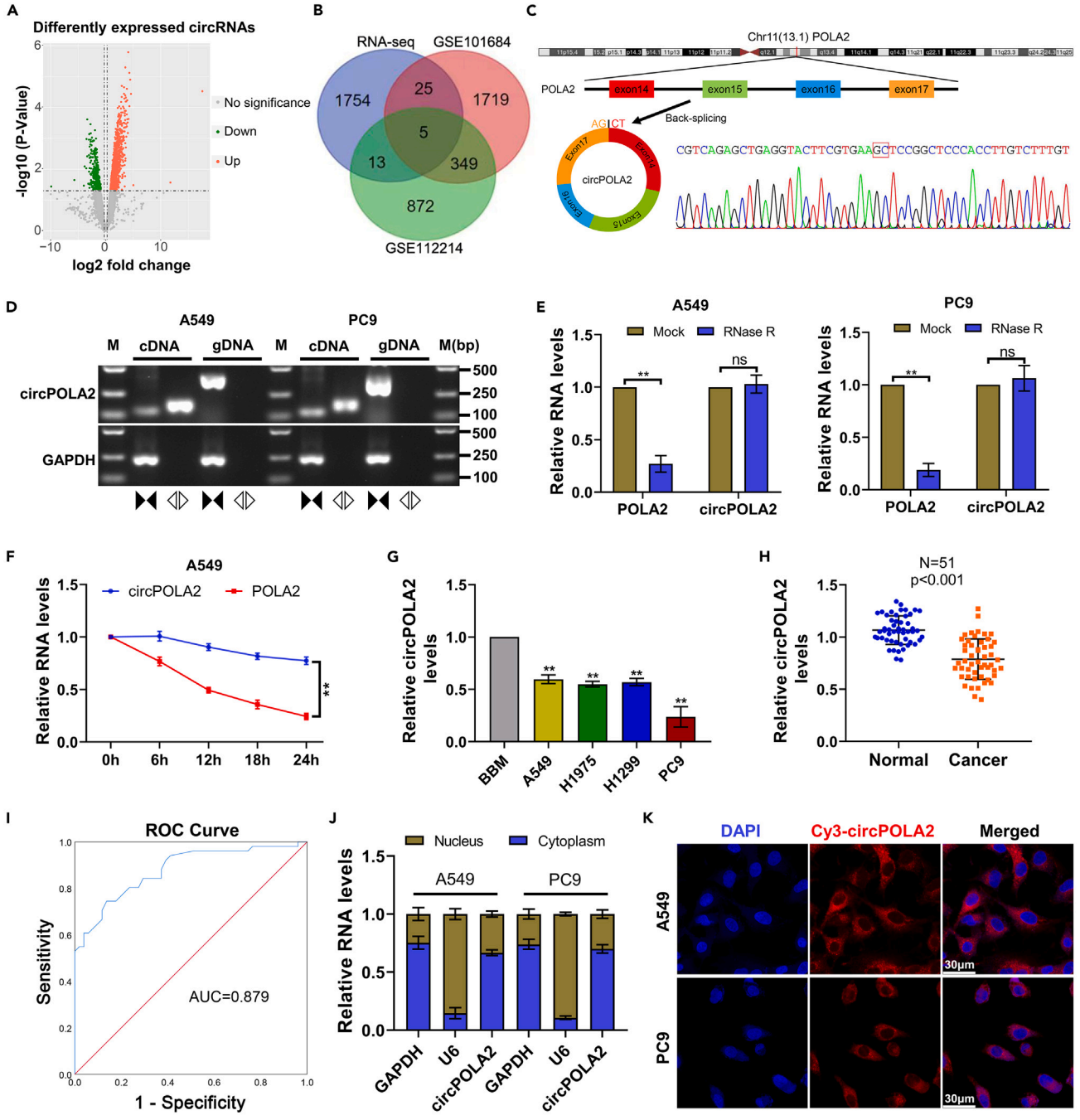

Figure 1. Identification and characterization of circPOLA2 in NSCLC

(A) Volcano plots show all 1797 differentially expressed circRNAs filtered at $p \leq 0.05$ in 4 paired NSCLC tissues and matched normal tissues.

(B) Venn diagram showing that 5 circRNAs were overlapped by our RNA-Seq data and two GEO datasets (GSE101684 and GSE112214).

(C) Schematic diagram shows the genomic location of circPOLA2 and the back-splicing site confirmed by Sanger sequencing.

(D) PCR with divergent or convergent primers and agarose gel electrophoresis demonstrated the presence of circPOLA2 and linear POLA2 in A549 and PC9 cells.

(E and F) The stability of circPOLA2 and linear POLA2 was tested by RT-qPCR after treatment with RNase R (E) and actinomycin D (F).

(G) Relative circPOLA2 levels in different NSCLC cell lines and normal bronchial epithelial cells were measured by RT-qPCR.

(H) Relative circPOLA2 levels in 51 paired NSCLC tissues and adjacent normal tissues were measured by RT-qPCR.

(I) ROC curve analysis was used to evaluate the diagnostic value of circPOLA2 for NSCLC (n = 102).

Figure 1. *Continued*

(J) Nuclear-cytoplasmic fractionation and RT-qPCR assays indicated that circPOLA2 was mainly distributed in the cytoplasmic of NSCLC cells; U6 and GAPDH genes were used as nuclear and cytoplasmic controls, respectively.

(K) RNA-FISH shows the cytoplasm localization of circPOLA2; the circPOLA2 probe was labeled with Cy3 (red), while nuclei were stained with DAPI (blue); scale bar: 20 μm. Data are presented as the mean ± SD (n = 3 per group, unless otherwise indicated). *$p < 0.05$, **$p < 0.01$, ***$p < 0.001$, ns: not significant.

See also Table S4.

The Hippo signaling pathway is a well-characterized tumor suppressor signaling network, the key components of which include mammalian STE20-like kinase 1/2 (MST1/2), Salvador homolog 1 (SAV1), large tumor suppressor kinase 1/2 (LATS1/2), Yes-associated protein 1 (YAP) and transcriptional coactivator with PDZ-binding motif (TAZ), as well as upstream regulators, such as the activator Merlin (product of the NF2 gene) and the inhibitor striatin (STRN)-interacting phosphatase and kinase (STRIPAK) complex.[20] Once activated, the effectors' YAP and TAZ are phosphorylated by LATS1/2 and sequestered in the cytoplasm by 14-3-3 proteins, thereby inhibiting the oncogenic effect of YAP/TAZ in cancers, including NSCLC.[20,21] There are currently two opposing views on the role of YAP/TAZ in ferroptosis in cancer. On the one hand, TAZ has been reported to induce ferroptosis in renal cell carcinoma[22] and epithelial ovarian cancer,[23] while YAP has been shown to promote ferroptosis in mesothelioma cells.[24] On the other hand, YAP/TAZ has been reported to prevent ferroptosis in hepatocellular carcinoma.[25] Recently, a team reported that YAP increased ferroptosis resistance in NSCLC cells by interacting with the transcription factor CP2 (TFCP2) and promoting the transcription of ferritin heavy chain 1 (FTH1)[26] and ferritin light chain 1 (FTL1).[27] However, further studies are needed to validate the modulatory effect of YAP on ferroptosis in NSCLC.

In this study, we identified a downregulated circRNA, circPOLA2 (hsa_circ_0004291), in NSCLC tissues by RNA-Seq and bioinformatics analysis. We then found that circPOLA2 was negatively correlated with clinical stage, sensitized NSCLC cells to ferroptosis and suppressed tumorigenesis both *in vitro* and *in vivo*. Mechanistically, circPOLA2 interacts with Merlin and restricts its phosphorylation at S518, leading to the activation of the Hippo pathway and the inhibition of YAP in NSCLC. Our results suggest that circPOLA2 may be a novel therapeutic target and a promising biomarker for NSCLC.

RESULTS

CircPOLA2 expression was downregulated in non-small cell lung cancer and negatively correlated with clinical stage

To screen for circRNAs that contribute to NSCLC progression, 4 pairs of NSCLC and adjacent normal lung tissues were used for RNA-Seq analysis. Among all 13,821 predicted circRNAs, 1,797 circRNAs were judged to be differentially expressed by the cutoff criteria $p \leq 0.05$ (Figure 1A; Table S4). Differentially expressed circRNAs in two GEO datasets (GSE101684 and GSE112214), which contain microarray expression profiles of circRNAs in NSCLC and matched normal lung tissues were downloaded and analyzed. Using the same criteria ($p \leq 0.05$), 2098 and 1239 differentially expressed circRNAs were identified in the GSE101684 and GSE112214 datasets respectively. Taking the intersection of our RNA-Seq results with these two GEO datasets, 5 overlapping circRNAs (hsa_circ_0089974, hsa_circ_0025506, hsa_circ_0006857, hsa_circ_0004291, and hsa_circ_0002017) were found (Figure 1B; Table S4). However, only hsa_circ_0004291 was consistently downregulated in the three datasets, so we selected it for further study and renamed it circPOLA2. According to circBase[28] annotation, circPOLA2 (chr11:65061623-65063461) is back-spliced from exons 14–17 of the POLA2 gene. The back-splicing junction site was verified by Sanger sequencing (Figure 1C). To further confirm that circPOLA2 is generated by head-to-tail splicing, convergent and divergent primers were used to amplify circPOLA2 and linear POLA2 transcripts. Electrophoresis of the PCR products revealed that circPOLA2 could be amplified from cDNA only by the divergent primers, whereas the convergent primers produced corresponding fragments of POLA2 from both cDNA and gDNA templates (Figure 1D). As expected, circPOLA2 showed higher stability than the linear POLA2 transcript when treated with RNase R or actinomycin D in NSCLC cells (Figures 1E and 1F).

To explore the clinical significance of circPOLA2, we first examined the expression of circPOLA2 in NSCLC cell lines and tissues by RT-qPCR. The results showed that circPOLA2 levels were lower in NSCLC cells than in normal bronchial epithelial cells (BBM) (Figure 1G). Moreover, circPOLA2 expression was significantly lower in cancer tissues than in matched normal tissues (Figure 1H). A receiver operating characteristic (ROC) curve was plotted to assess the diagnostic value of circPOLA2 for NSCLC. The area under the curve was 0.879, and the specificity and sensitivity were 86.3% and 74.5%, respectively, with a cutoff value of 0.925 (Figure 1I). In addition, we found that circPOLA2 expression was negatively correlated with N stage, TNM stage, and histological grade but not with other clinical parameters (Table 1). To determine the subcellular localization of circPOLA2, we first performed a nuclear-cytoplasmic fractionation assay and found that circPOLA2 was predominantly localized in the cytoplasm of NSCLC cells (Figure 1J). This finding was further confirmed by the RNA-FISH assay (Figure 1K). Taken together, these data implied that circPOLA2 expression was downregulated in NSCLC cell lines and tissues and negatively correlated with clinical stage, suggesting that circPOLA2 may function as a tumor suppressor.

CircPOLA2 suppressed the proliferation and aggressiveness of non-small cell lung cancer cells *in vitro*

To explore the function of circPOLA2 in NSCLC cells, we first constructed circPOLA2 overexpression or silencing plasmids and transfected them into A549 and PC9 cells. Stably transfected cell lines were obtained, and the efficiency of overexpression and knockdown was validated by RT-qPCR while having little impact on the expression of linear POLA2 mRNA (Figure 2A). Then, a series of cell function experiments were performed. The CCK-8 and EdU incorporation assays indicated that circPOLA2 overexpression reduced cell proliferation ability compared to the control group, while circPOLA2 knockdown had the opposite effect (Figures 2B–2D). The colony formation experiment indicated that

Table 1. Correlation between circPOLA2 expression and clinicopathological features in 51 patients with NSCLC

		circPOLA2[c]				Spearman correlation	
Characteristic	All cases	Low	High	Chi-square	*p* values	Coefficient	*p* values
All cases	51	26	25				
Gender						0.057	0.690
Male	31	16	15	0.013	0.910		
Female	20	10	10				
Age						0.108	0.452
≤60years	18	11	7	1.142	0.285		
>60years	33	15	18				
T stage						−0.247	0.080
T1	31	12	19	4.763	0.029*		
T2-3	20	14	6				
N stage							
N0	36	12	24	15.253	<0.001***	−0.691	<0.001***
N1-2	15	14	1				
TNM stage						−0.767	<0.001***
I	31	8	23	20.046	<0.001***		
II-III	20	18	2				
Histological grade[a]						−0.512	<0.001***
1	7	1	6	7.299[b]	0.027*		
2	21	9	12				
3 + 4	23	16	7				

*$P < 0.05$, **$P < 0.01$, ***$P < 0.001$.

[a]1 = well differentiated, 2 = moderately differentiated, 3 = poorly differentiated, 4 = undifferentiated.

[b]Fisher's Exact Test.

[c]The median of relative circPOLA2 expression is 0.76, and was used as the cut-off value for grouping (High>0.76; Low≤0.76).

circPOLA2 overexpression decreased the colony formation ability compared to the control group, while circPOLA2 knockdown promoted colony formation in both cell lines (Figures 2E and 2F). Transwell assays showed that circPOLA2 overexpression markedly reduced migration and invasion, whereas circPOLA2 knockdown increased cell aggressiveness (Figures 2G and 2H). Additionally, we noted that circPOLA2-sh1 had a slightly stronger effect than circPOLA2-sh2 in the above cell functional experiments, although the difference did not reach statistical significance. In conclusion, these data demonstrated that circPOLA2 exerts a tumor-suppressive effect in NSCLC *in vitro*.

CircPOLA2 sensitized non-small cell lung cancer cells to ferroptosis *in vitro* and suppressed tumorigenesis *in vivo*

Ferroptosis is an iron-dependent form of RCD that has been implicated in the progression and therapeutic responses of several cancers, including NSCLC, and the induction of ferroptosis may be a promising therapeutic strategy for certain cancers.[8,29] Noncoding RNAs, including circRNAs, have been reported to regulate ferroptosis in various types of cancer.[19] We, therefore, asked whether circPOLA2 could modulate ferroptosis in NSCLC progression. We first evaluated the sensitivity to erastin-induced ferroptosis by measuring intracellular ATP levels, which indicate cell viability. The results showed that circPOLA2 overexpression significantly increased the sensitivity to the erastin-induced decrease in cell viability in both A549 and PC9 cells (Figure 3A). The increased sensitivity to erastin in circPOLA2 overexpressing NSCLC cells could be rescued by the ferroptosis inhibitors ferrostatin-1 (Fer-1) and DFO (Figure 3B). However, inhibitors of other forms of cell death, including apoptosis (Z-VAD-FMK), autophagy (3-MA), and necroptosis (necrostatin-1, Nec-1), failed to rescue the erastin-induced decline in cell viability (Figure 3B). This suggests that the type of cell death induced by erastin in NSCLC cells was predominantly ferroptosis rather than apoptosis, autophagy, or necroptosis. Flow cytometry analysis of dead cells also showed that overexpression of circPOLA2 promoted erastin-induced cell death and that Fer-1 and DFO significantly attenuated erastin-induced cell death (Figures S1A and 1B). Iron-catalyzed peroxidation of PUFA-PLs is the execution step of ferroptosis, and the accumulation of lipid peroxides is a cardinal feature of ferroptosis.[8] The lipophilic fluorescent probe BODIPY 581/591 C11 was used to detect lipid peroxides. The results indicated that circPOLA2 overexpression increased the level of lipid peroxides triggered by erastin in NSCLC cells, whereas inhibitors of ferroptosis abolished the effect of erastin (Figures 3C, 3D, and S1C). Malondialdehyde (MDA) content showed a similar change to lipid peroxidation (Figure 3E). TEM imaging revealed that the mitochondria in circPOLA2-overexpressing PC9 cells exhibited typical morphological features of ferroptosis after erastin treatment, including smaller size, increased membrane density, and reduced number of cristae (Figure 3F). Additionally, table overexpression

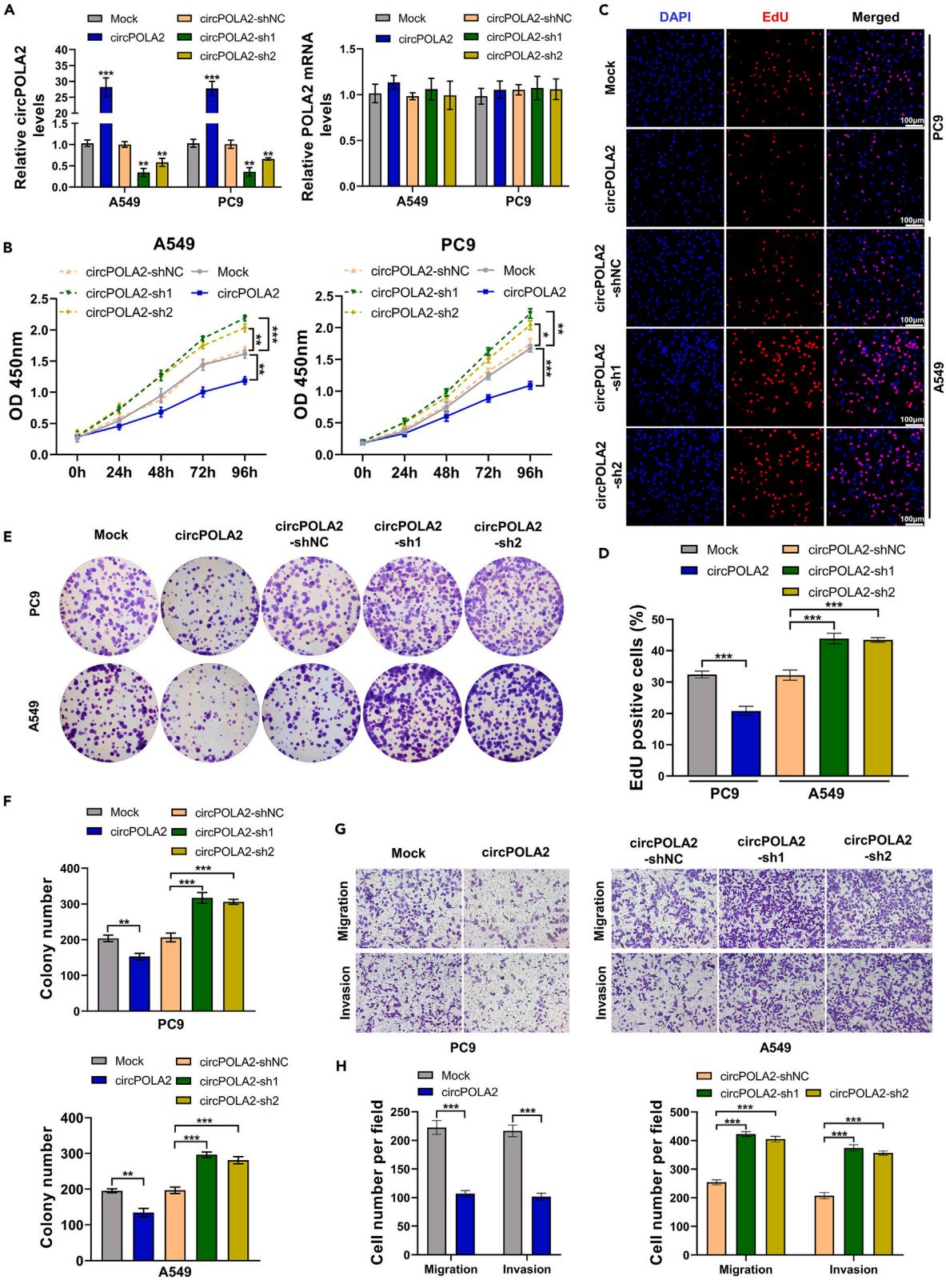
A
Mock
circPOLA2
circPOLA2-shNC
circPOLA2-sh1
circPOLA2-sh2
Relative circPOLA2 levels
Relative POLA2 mRNA levels
A549
PC9
B
A549
PC9
OD 450nm
0h
24h
48h
72h
96h
C
DAPI
EdU
Merged
Mock
circPOLA2
circPOLA2 -shNC
circPOLA2 -sh1
circPOLA2 -sh2
100μm
D
EdU positive cells (%)
E
F
Colony number
G
Migration
Invasion
H
Cell number per field

Figure 2. CircPOLA2 suppressed the proliferation and aggressiveness of NSCLC cells *in vitro*

(A) RT-qPCR measured the relative expression of circPOLA2 and linear POLA2 in A549 and PC9 cells stably transfected with circPOLA2 overexpression or knockdown plasmid.

(B) Cell growth curves were plotted by CCK-8 assays after circPOLA2 overexpression or knockdown in A549 and PC9 cells.

(C and D) An EdU incorporation assay was used to evaluate proliferation; scale bar: 50 μm.

(E and F) Colony formation assay was used to assess cell survival and growth ability.

(G and H) Transwell assay was used to measure cell migration and invasion ability (magnification: ×100). Data are presented as the mean ± SD ($n = 3$ per group, unless otherwise indicated). *$p < 0.05$, **$p < 0.01$, ***$p < 0.001$.

of circPOLA2 obviously suppressed the growth of xenografts generated by the subcutaneous injection of PC9 cells into athymic nude mice (Figures 3G–3I). In conclusion, circPOLA2 sensitized NSCLC cells to ferroptosis *in vitro* and suppressed tumor growth *in vivo*.

CircPOLA2 interacted with merlin and activated the hippo signaling pathway

To research the molecular mechanism underlying the function of circPOLA2, we performed an RNA pull-down assay, followed by silver staining and mass spectrometry to identify the circPOLA2-binding proteins (Figures 4A and 4B). A total of 210 proteins (Table S3) were significantly enriched according to the filtering criteria fold change ≥ 1.5; these candidates were then intersected with ferroptosis regulators downloaded from an online database FerrDb.[30] Finally, 7 overlapping proteins were found: Merlin, TFAP2A, DAZAP1, HMOX1, LIG3, CISD2, and GJA1 (Figure 4C). Among them Merlin (product of the NF2 gene) was the most highly enriched, so we chose it for further validation via RIP followed by PCR. The results showed that both endogenous and overexpressed circPOLA2 were precipitated by an anti-Merlin antibody but not the IgG control (Figures 4D and 4E). Subsequently, FISH and IF double staining confirmed the cytoplasmic colocalization of circPOLA2 and Merlin (Figure 4F). Merlin is a potent upstream activator of the Hippo pathway and contributes to the recruitment of core Hippo kinase modules.[31,32] To identify the binding domain between Merlin and circPOLA2, a series of Flag-tagged truncated forms of Merlin were designed and overexpressed in A549 cells.[33] The RIP-PCR assay indicated that the C-terminal domain but not the other domains of Merlin is crucial for binding to circPOLA2 (Figure 4G).

As a well-known tumor suppressor, the activity of Merlin requires a closed conformation formed by the intramolecular association between the FERM domain and the C-terminal domain; the closed conformation is converted to an open conformation (inactive form) when S518 is phosphorylated by p21-activated kinase (PAK).[33] Our results showed that circPOLA2 could bind to the C-terminal domain of Merlin which contains S518. We therefore hypothesized that circPOLA2 might regulate the Hippo pathway by affecting the phosphorylation of Merlin at S518. To test this hypothesis, we first measured the phosphorylation levels of Merlin (Ser518), Lats1 (Thr1079), and YAP (Ser127) in NSCLC cells stably transfected with circPOLA2 overexpression or knockdown plasmids by WB. The results revealed that the level of p-Merlin (Ser518) was significantly reduced by circPOLA2 overexpression and increased by circPOLA2 knockdown. Conversely, the levels of *p*-Lats1 (Thr1079) and p-YAP (Ser127) were increased in the circPOLA2 overexpression group and decreased in the circPOLA2 knockdown group (Figure 5A). Moreover, total YAP expression was slightly decreased and increased in circPOLA2-overexpressing and circPOLA2-silenced cells, respectively, whereas total Merlin and total Lats1 expression showed little change in the different groups (Figure 5A). To further verify the role of circPOLA2 in the Hippo signaling pathway, we also measured the expression of classical oncogenes[21] (CTGF, CYR61, AREG, and MYC) downstream of YAP via RT-qPCR. The results revealed that these four genes were significantly downregulated and upregulated in circPOLA2-overexpressing and circPOLA2-silenced NSCLC cells, respectively (Figure 5B). To confirm the necessity of Merlin in mediating the role of circPOLA2 in Hippo pathway activation, we performed bidirectional rescue experiments; specifically, we silenced Merlin in circPOLA2-overexpressing PC9 cells and overexpressed a constitutively activated Merlin mutant (S518A)[34] in circPOLA2-silenced A549 cells. The reliability and efficiency of the gene manipulation strategies were validated by RT-qPCR (Figures S2A and 2B). The results showed that Merlin silencing markedly attenuated the Hippo pathway activation triggered by circPOLA2 overexpression and rescued the reduction in the expression of CTGF, CYR61, AREG, and MYC (Figures 5C and 5E). In contrast, overexpression of mutant Merlin (S518A) significantly reversed the inhibitory effect of circPOLA2 silencing on the Hippo pathway and reversed the elevation of the expression of CTGF, CYR61, AREG, and MYC (Figures 5D and 5F). Additionally, silencing Merlin and overexpressing mutant Merlin (S518A) alone dramatically inhibited and activated the Hippo pathway, respectively (Figures 5C–5F). Collectively, these data suggest that circPOLA2 interacts with Merlin, preventing its phosphorylation at S518 and further activating the Hippo signaling pathway in NSCLC cells.

CircPOLA2 regulated the ferroptosis sensitivity and tumorigenicity of non-small cell lung cancer cells via merlin

To verify the necessity of Merlin for the regulatory effect of circPOLA2 on the ferroptosis sensitivity and tumorigenicity of NSCLC cells, we performed a series of rescue experiments. First, the proliferation, colony formation, aggressiveness, and ferroptosis sensitivity of PC9 cells stably cotransfected with circPOLA2 overexpression and Merlin silencing vectors were tested. The CCK-8 and EdU incorporation assays indicated that Merlin knockdown dramatically reversed the inhibition of cell proliferation induced by circPOLA2 overexpression (Figures 6A–6C). The suppression of the colony formation, migration, and invasion of circPOLA2-overexpressing cells was also obviously reversed by Merlin silencing (Figures 6D and 6E). Intracellular ATP levels indicated that Merlin knockdown significantly reversed the sensitization to ferroptosis triggered by circPOLA2 overexpression (Figure 6F). Consistently, Merlin knockdown reversed the elevation of lipid peroxidation and MDA levels triggered by circPOLA2 overexpression (Figures 6G and 6H). Additionally, the typical mitochondrial morphological changes induced by erastin in circPOLA2-overexpressing PC9 cells were also abolished by Merlin silencing (Figure 6I). Second, the same experiments were performed in A549 cells with circPOLA2 knockdown and Merlin (S518A) overexpression. The results indicated that cell proliferation, colony

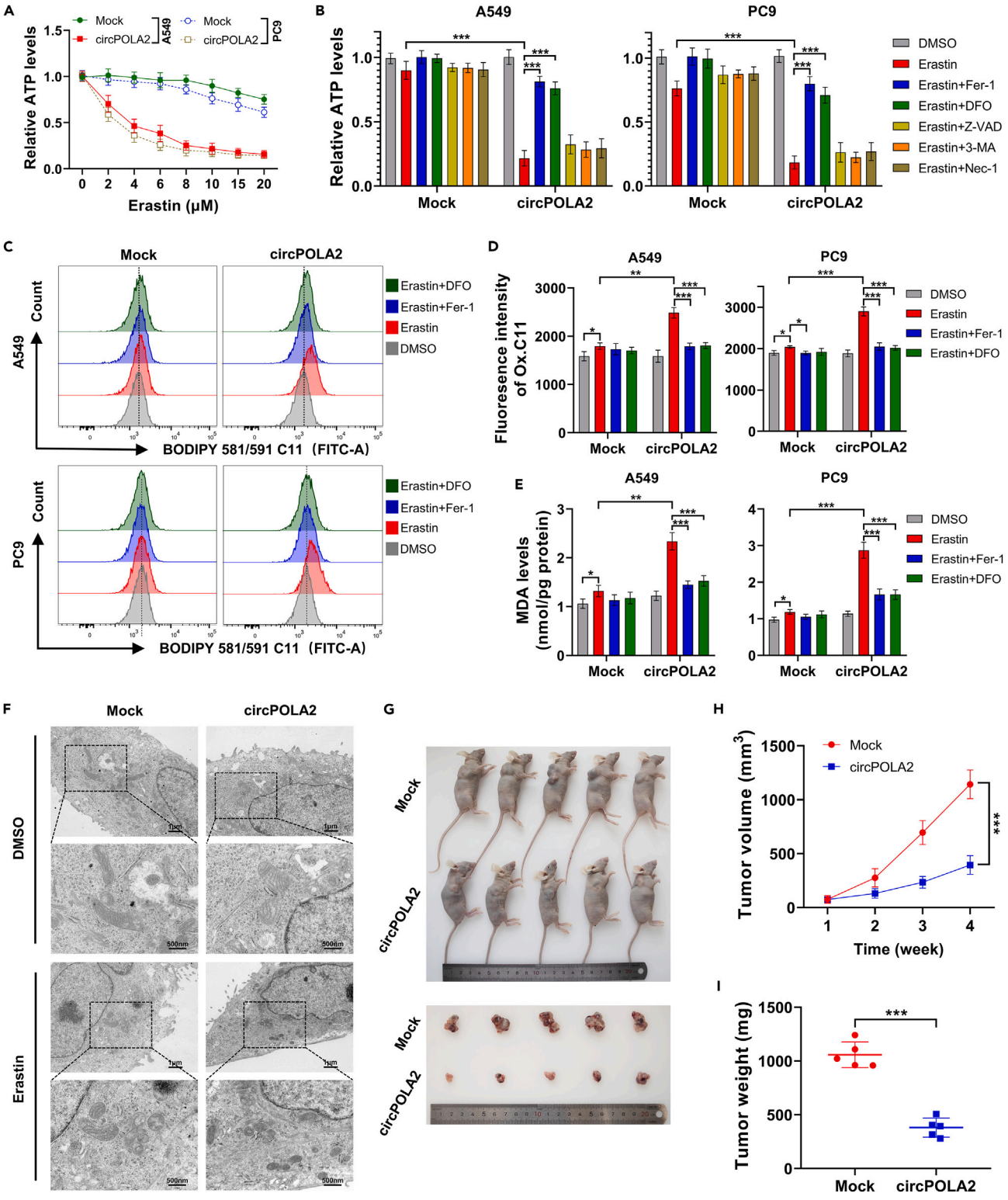

Figure 3. CircPOLA2 sensitized NSCLC cells to ferroptosis *in vitro* and suppressed tumorigenesis *in vivo*

(A–E) A549 and PC9 cells with or without circPOLA2 overexpression were treated with erastin (10 μmol/L or indicated concentration) or erastin plus Fer-1 (1 μmol/L), DFO (50 μmol/L), Z-VAD (10 μmol/L), 3-MA (2 mmol/L), or Nec-1 (10 μmol/L) for 20 h.

(A) Intracellular ATP levels were measured after treatment with different concentrations of erastin.

Figure 3. *Continued*

(B) Intracellular ATP levels were measured after treatment with erastin (10 μmol/L) or erastin plus different cell death inhibitors.

(C and D) Representative flow cytometry histogram of lipid peroxides stained with BODIPY 581/591 C11 (C), and the statistical results of the mean fluorescence intensity of oxidized BODIPY 581/591 C11 (D).

(E) Intracellular MDA levels were measured by colorimetry, and the results were expressed as μmol per mg protein.

(F) TEM images of mitochondria from PC9 cells treated with erastin (10 μmol/L) or DMSO for 20 h.

(G–I) PC9 cells with stable circPOLA2 overexpression or negative control were injected into the dorsal flanks of nude mice (n = 5 per group); gross tumor appearance *in vivo* and *ex vivo* (G); *in vivo* growth curves were plotted by the tumor sizes measured weekly (H), and weight was measured at the endpoint (I). Data are presented as the mean ± SD (n = 3 per group, unless otherwise indicated). *$p < 0.05$, **$p < 0.01$, ***$p < 0.001$.

See also Figure S1.

formation, migration, and invasion were significantly promoted by circPOLA2 silencing, and these effects could be reversed by Merlin (S518A) overexpression (Figures S3A–S3E). Similarly, sensitivity to ferroptosis and the levels of lipid peroxidation and MDA were markedly increased by circPOLA2 knockdown, but these changes were reversed by overexpressing Merlin (S518A) (Figures S3F–S3I). Notably, circPOLA2 overexpression or knockdown also slightly suppressed or increased ferroptosis, respectively, in the absence of erastin treatment (Figures 6G–6I and S3G–S3I). In summary, circPOLA2 regulated the ferroptosis sensitivity and tumorigenesis of NSCLC cells via Merlin *in vitro*.

XMU-MP-1 reversed the effect of circPOLA2 on the ferroptosis sensitivity and tumorigenicity of non-small cell lung cancer cells

To further confirm that the effect of circPOLA2 on NSCLC cells was dependent on Hippo pathway activation, a Hippo pathway inhibitor, XMU-MP-1,[35] was used. We first validated the inhibitory effect of XMU-MP-1 on the Hippo pathway by measuring the level of p-YAP (Ser127) in PC9 cells (Figure S4A). Cell proliferation, colony formation, migration, and invasion were significantly inhibited by circPOLA2 overexpression, and these effects could be reversed by XMU-MP-1 treatment (Figures S4B–S4F). As indicated by the measurement of intracellular ATP levels, XMU-MP-1 treatment markedly reversed the increase in ferroptosis sensitivity induced by circPOLA2 overexpression (Figure S4G). Similarly, flow cytometry analysis of dead cells showed that XMU-MP-1 treatment dramatically reduced cell death in circPOLA2-overexpressing PC9 cells (Figures S4H and S4I). Consistently, the levels of lipid peroxidation and MDA were markedly increased by circPOLA2 overexpression, but these changes were reversed by XMU-MP-1 treatment (Figures S4J–S4L). Collectively, these data suggest that the effect of circPOLA2 on the ferroptosis sensitivity and tumorigenicity of NSCLC cells is dependent on the activation of the Hippo pathway.

CircPOLA2 sensitized non-small cell lung cancer cells to ferroptosis and inhibited tumorigenesis via merlin

To further test the necessity of Merlin in mediating the effect of circPOLA2 in NSCLC, we performed rescue experiments in a xenograft model established by injecting PC9 cells stably overexpressing circPOLA2 with or without Merlin knockdown. The results revealed that circPOLA2 overexpression or Merlin silencing suppressed or promoted xenograft growth, respectively; moreover, Merlin silencing reversed the tumor suppression effect of circPOLA2 overexpression (Figures 7A–7C). Ki-67 expression was analyzed by IHC to evaluate cell proliferation. The results showed that circPOLA2 overexpression reduced Ki-67 expression and that Merlin silencing significantly reversed the inhibition of Ki-67 expression triggered by circPOLA2 overexpression (Figures 7D and 7E). Both 4-hydroxynonenal (4-HNE) and MDA are the end products of lipid peroxidation, and are commonly used as biomarkers of lipid peroxidation.[36] We examined 4-HNE and MDA levels in xenograft tumors by IHC staining and colorimetric methods, respectively. The results showed that circPOLA2-overexpressing tumors had increased 4-HNE staining and MDA levels compared to control tumors, while this increase was reversed by Merlin silencing (Figures 7F–7H). Taken together, these data imply that Merlin mediates the effect of circPOLA2 on ferroptosis sensitivity and tumor suppression in NSCLC *in vivo*.

Finally, to verify the existence of the circPOLA2/Merlin/Hippo pathway in clinical NSCLC samples, we tested the Hippo pathway activity in 5 paired cancer and adjacent normal tissues from patients with NSCLC by WB. The results showed that the Hippo pathway activity of the cancer tissues was significantly lower than that of the paired normal tissues (Figure S5). This was consistent with the decreased expression of circPOLA2 in cancer tissues (Figure 2H). Therefore, this result further supports the pivotal regulatory role of the circPOLA2/Merlin/Hippo pathway in NSCLC progression.

DISCUSSION

To provide new insights into the tumorigenesis of NSCLC, we identified a significantly downregulated cytoplasmic circRNA, circPOLA2, in NSCLC. By overexpressing or silencing circPOLA2, we found that circPOLA2 restrained NSCLC cell proliferation, migration, invasion, and xenograft tumor growth. In addition, circPOLA2 dramatically promoted NSCLC cell ferroptosis induced by erastin. Mechanistic studies showed that circPOLA2 binds to the C-terminal region of Merlin and restricts its phosphorylation at S518, leading to the activation of the Hippo signaling pathway. Subsequently, a reduction in active YAP mediated the ferroptosis-sensitizing and tumor-suppressive effects of circPOLA2.

The vast majority of circRNAs accumulate in the cytoplasm, and miRNA sponging is the most commonly postulated function of circRNAs.[5] However, most circRNAs contain few miRNA binding sites and are expressed at low levels,[37,38] making them unlikely to function as miRNA sponges or as competing endogenous RNAs.[39] An increasing number of studies have shown that circRNAs function by interacting with proteins in both the nucleus and cytoplasm.[40] For example, circ-CTNNB1 interacts with the m6A regulator RBM15 and increases m6A levels of key

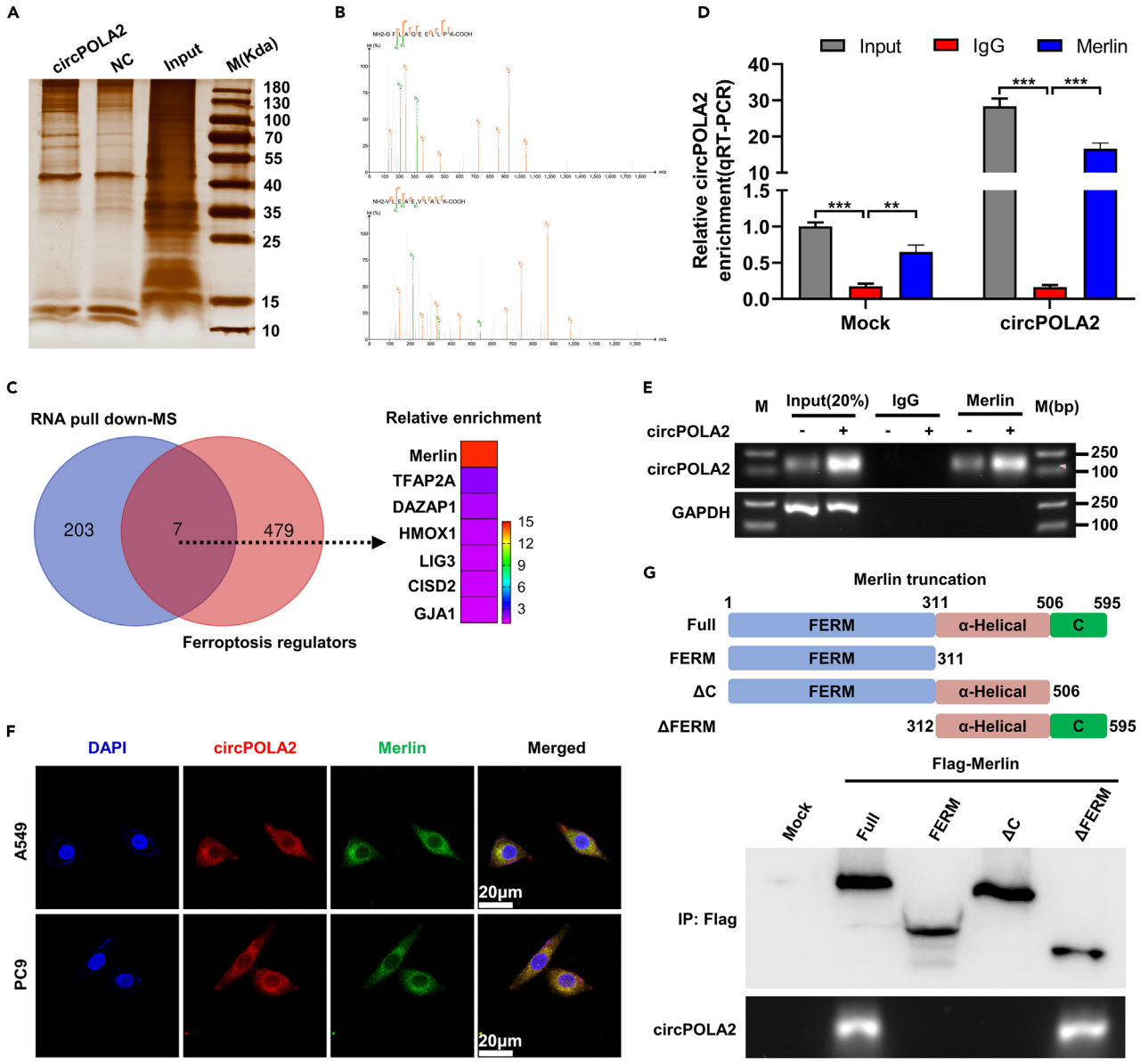

Figure 4. CircPOLA2 directly interacted with Merlin

(A and B) RNA pull-down assay was performed using the biotin-labeled antisense or sense (negative control) probes for the cirPOLA2 back-splicing site; the protein products were used for silver staining (A) and mass spectrometry (MS) analysis (B).

(C) Venn diagram showing that 7 proteins overlapped with our MS data and ferroptosis regulators.

(D and E) RIP experiments were performed in A549 cells with or without circPOLA2 overexpression using anti-Merlin antibody or IgG control; the enrichment of circPOLA2 was detected by RT-qPCR (D) or RT-PCR followed by agarose gel electrophoresis (E).

(F) FISH and IF double staining shows the colocalization of circPOLA2 (red) and Merlin (green) in A549 and PC9 cells; nuclei were stained with DAPI (blue); scale bar: 20 μm.

(G) Schematic diagram showing the design of the truncated Merlin (top panel); RIP assay using anti-Flag antibody was performed to validate the binding domain of Merlin with circPOLA2 (bottom panel). Data are presented as the mean ± SD (n = 3 per group). *p < 0.05, **p < 0.01, ***p < 0.001.

See also Table S3.

glycolysis gene transcripts, thereby promoting aerobic glycolysis and tumorigenesis in osteosarcoma cells[41]; circPTPRA suppresses bladder cancer progression by binding to IGF2BP1 and inhibiting its interaction with downstream m6A-modified mRNAs (MYC and FSCN1)[42]; and circNDUFB2 has been found to act as a tumor suppressor in NSCLC by mediating the interaction between TRIM25 and IGF2BPs, thereby facilitating the ubiquitination and degradation of IGF2BPs.[43] In this study, we found that circPOLA2 interacts with Merlin in the cytoplasm. Furthermore, the C-terminal region of Merlin is essential for its interaction with circPOLA2.

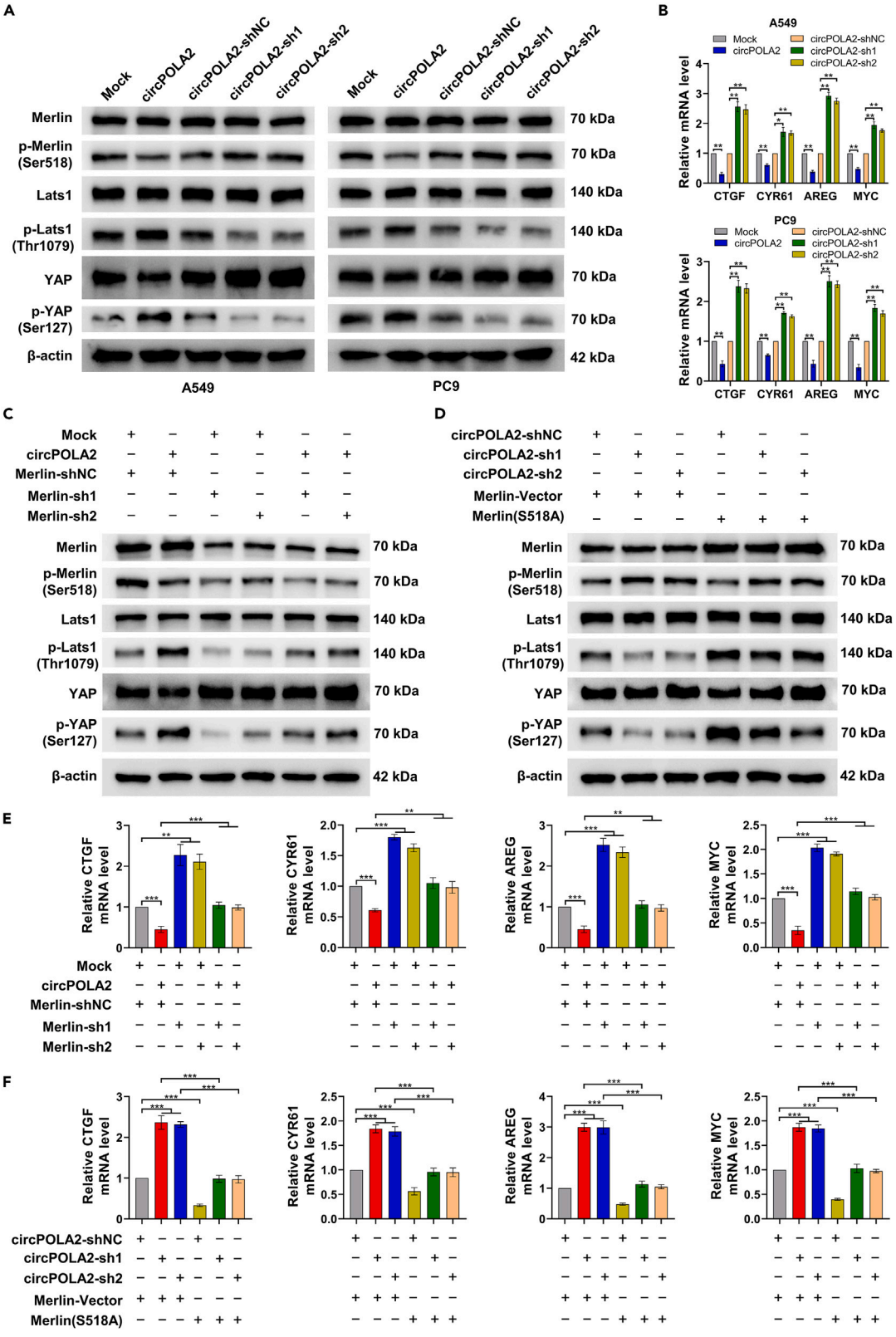
A
Mock
circPOLA2
circPOLA2-shNC
circPOLA2-sh1
circPOLA2-sh2
Merlin
p-Merlin (Ser518)
Lats1
p-Lats1 (Thr1079)
YAP
p-YAP (Ser127)
β-actin
70 kDa
140 kDa
42 kDa
A549
PC9
B
A549
PC9
Relative mRNA level
CTGF
CYR61
AREG
MYC
C
D
circPOLA2-shNC
circPOLA2-sh1
circPOLA2-sh2
Merlin-Vector
Merlin(S518A)
E
F
Relative CTGF mRNA level
Relative CYR61 mRNA level
Relative AREG mRNA level
Relative MYC mRNA level

Figure 5. CircPOLA2 activated the Hippo signaling pathway by inhibiting the phosphorylation of Merlin

(A) Representative WB results show Hippo pathway activity in NSCLC cells with circPOLA2 overexpression or knockdown.

(B) The expression levels of classical oncogenes downstream of YAP were measured by RT-qPCR.

(C–F) Bidirectional rescue experiments were performed to examine the necessity of Merlin. Specifically, we silenced Merlin in circPOLA2-overexpressing PC9 cells and overexpressed a constitutively activated Merlin mutant (S518A) in circPOLA2-silenced A549 cells. Representative WB results showing Hippo pathway activity (C, D); the expression of classical oncogenes downstream of YAP was measured by RT-qPCR (E, F). Data are presented as the mean ± SD (n = 3 per group). *$p < 0.05$, **$p < 0.01$, ***$p < 0.001$.

See also Figure S2.

Dysregulation of the Hippo pathway is an important cause of many malignancies, including NSCLC.[20,21] Merlin is a potent upstream activator of the Hippo pathway and contributes to the recruitment of core Hippo kinases.[31,32] Similar to the other members of the ERM family of proteins, Merlin is composed of an N-terminal FERM domain, an intermediate coiled-coil segment, and a C-terminal domain. However, unlike other canonical ERM proteins, Merlin maintains an active state by intramolecular association between the FERM domain and the C-terminal tail. The transition between the closed (active form) and open (inactive form) conformations is primarily controlled by the phosphorylation or dephosphorylation of S518 in the C-terminal domain, which is induced by mitogenic or antimitogenic signals, respectively.[33,44] Consistent with previous theories, we found that circPOL2 interacts with the C-terminal domain of Merlin and interferes with the phosphorylation of S518, leading to the activation of the Hippo pathway. The transcriptional coactivators YAP and TAZ are the final effectors of the Hippo pathway[20] and we found that p-YAP (S127) levels were significantly increased by circPOLA2 overexpression, while the expression of classical oncogenes[21] (CTGF, CYR61, AREG, and MYC) downstream of YAP/TAZ was reduced by circPOLA2 overexpression. These downregulated oncogenes partly account for the tumor suppressive effects of circPOLA2 in NSCLC. As mentioned above, phosphorylation at S518 drives the active-inactive cycle of Merlin, and mutation of S518 to alanine (S518A) has been demonstrated to mimic dephosphorylated Merlin.[34] Consistently, our results showed that overexpression of mutant Merlin (S518A) reversed the inhibition of the Hippo pathway induced by circPOLA2 knockdown. Taken together, these results suggest that circPOLA2 activates the Hippo pathway by binding to Merlin and inhibiting its phosphorylation at S518.

Targeting ferroptosis is a promising strategy for the treatment of cancer, including NSCLC.[8,45] Tumors have developed at least three strategies to escape ferroptosis and facilitate tumorigenesis, including limiting PUFA-PL synthesis and peroxidation, reducing the availability of labile iron, and increasing cellular defenses against ferroptosis.[8] Targeting these ferroptosis evasion mechanisms represents a future direction for the development of ferroptosis-inducing cancer treatments. As the final effectors of the Hippo pathway, YAP/TAZ have been reported to repress ferroptosis in hepatocellular carcinoma cells through the TEAD/ATF4-SLC7A11 axis.[25] Recently, two studies have reported that YAP promotes ferroptosis resistance in NSCLC cells by interacting with the transcription factor CP2 (TFCP2), promoting the transcription of ferritin heavy chain 1 (FTH1)[26] and ferritin light chain 1 (FTL1)[27] and further reducing intracellular labile iron levels. Our present study supports this view, as the results show that YAP inhibition induced by circPOLA2 or mutant Merlin (S518A) overexpression markedly promoted lipid peroxidation and ferroptotic cell death in NSCLC cells, whereas the activation of YAP by circPOLA2 or Merlin knockdown significantly increased ferroptosis resistance. In addition, the Hippo pathway inhibitor XMU-MP-1 reversed the effect of circPOLA2 on the ferroptosis sensitivity and tumorigenicity of NSCLC cells. However, several studies have suggested an opposite role for YAP/TAZ in regulating ferroptosis in cancer cells. For example, one team reported that TAZ induces ferroptosis in renal cell carcinoma[22] and epithelial ovarian cancer[23] through the EMP1-NOX4 and ANGPTL4-NOX2 axes, respectively. Another team reported that YAP promotes ferroptosis by upregulating several ferroptosis suppressors, including SLC7A11 and TFRC, in mesothelioma cells.[24] These seemingly contradictory observations may suggest that the role of YAP/TAZ in ferroptosis depends on the specific cellular context and the transcription factors to which they bind.[46]

In summary, we identified that circPOLA2 was downregulated in NSCLC tissues and cells, and we found that reduced circPOLA2 expression was correlated with advanced clinical stage in patients with NSCLC. We demonstrated that overexpression of circPOLA2 could inhibit the proliferation and aggressiveness of NSCLC cells and increase lipid peroxidation and ferroptotic cell death. Mechanistically, we discovered that circPOLA2 binds to the C-terminal domain of Merlin and restricts its phosphorylation at S518, leading to the activation of the Hippo signaling pathway. Although the exact role and mechanism of YAP/TAZ in regulating ferroptosis require further investigation, our results suggest that YAP enhances ferroptosis resistance in NSCLC cells both *in vitro* and *in vivo*. Our study provides new insights into the role of circRNAs in modulating ferroptosis and indicates that targeting the circPOLA2-Merlin-YAP axis is a promising therapeutic strategy for NSCLC.

Limitations of the study

The upstream mechanism of circPOLA2 downregulation needs further investigation. Although previous studies have shown that YAP could promote ferroptosis resistance in NSCLC by increasing the expression of FTH1 and FTL1, this was not tested in our study; moreover, whether other mechanisms involved in the regulatory role of YAP on ferroptosis remain unclear. YAP and TAZ are paralog transcriptional regulators, but they also have distinctive features; whether TAZ has the same effect as YAP in regulating ferroptosis sensitivity in NSCLC has not been validated in our study.

RESOURCE AVAILABILITY

Lead contact

Further information and requests for resources and reagents should be directed to and will be fulfilled by the lead contact, Jian Tang (tangjianku@yeah.net).

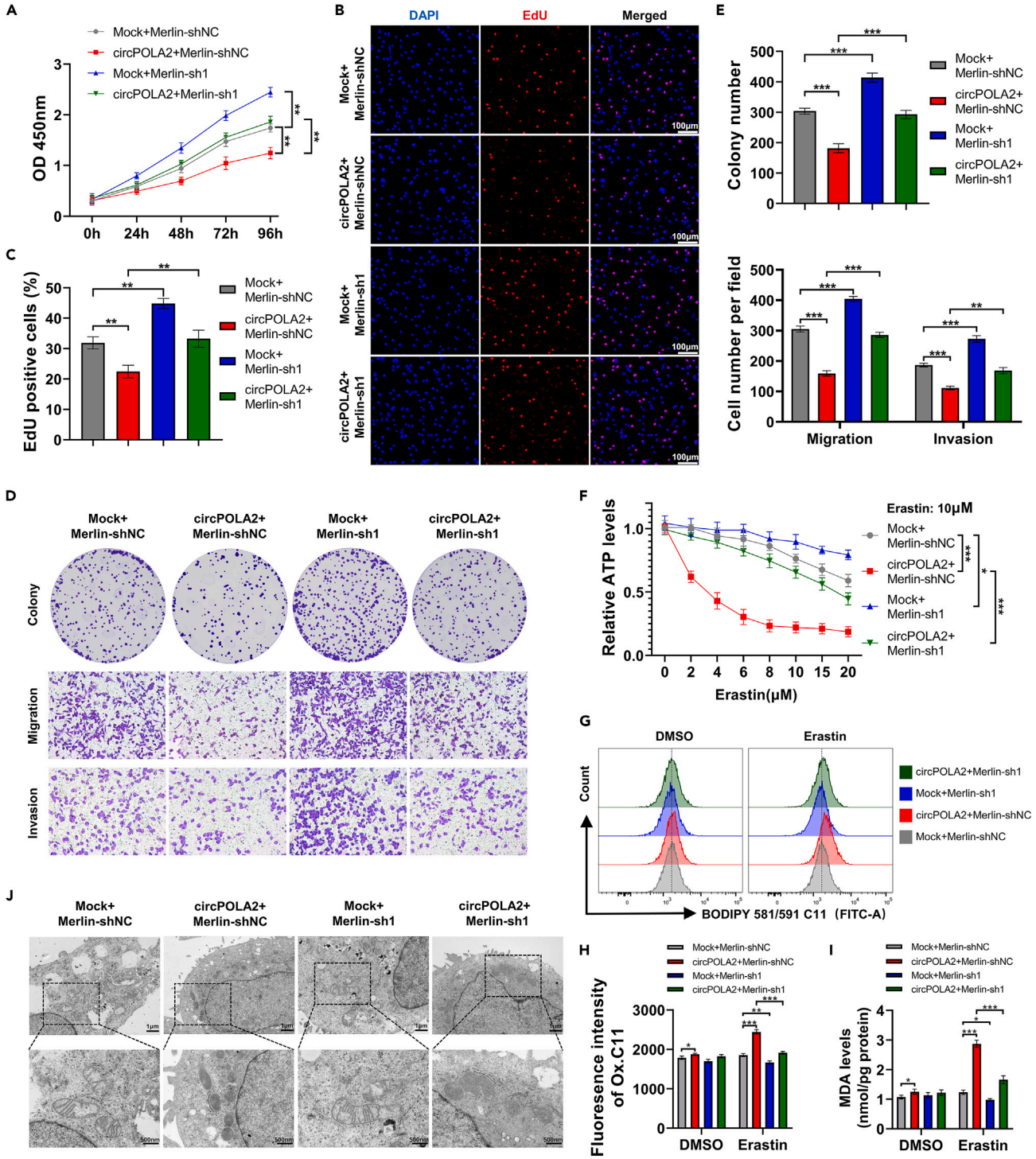

Figure 6. CircPOLA2 regulated the ferroptosis sensitivity and tumorigenicity of NSCLC cells via Merlin

CircPOLA2-overexpressing or empty vector was cotransfected with plasmids expressing Merlin-shRNAs or shNC into PC9 cells, and stably transfected cells were obtained for experiments.

(A) Cell growth curves were plotted using CCK-8 assays.

(B and C) An EdU incorporation assay was used to evaluate proliferation ability; scale bar: 50 μm.

(D and E) Colony formation, migration, and invasion assays were used to assess cell growth and aggressiveness (original magnification in Transwell assays: ×100).

(F) Intracellular ATP levels were measured after treatment with different concentrations of erastin for 20 h.

Figure 6. *Continued*

(G–I) Cells were treated with erastin (10 μmol/L) or DMSO for 20 h; representative flow cytometry histogram of lipid peroxides stained with BODIPY 581/591 C11 (G), and the statistical results of the mean fluorescence intensity of oxidized BODIPY 581/591 C11 (H); intracellular MDA levels were measured by colorimetry, and the results were expressed as μmol per mg protein (I).

(J) TEM images of mitochondria from PC9 cells treated with erastin (10 μmol/L) for 20 h. Data are presented as the mean ± SD (n = 3 per group). *$p < 0.05$, **$p < 0.01$, ***$p < 0.001$.

See also Figures S3 and S4.

Materials availability

This study did not generate new unique reagents.

Data and code availability

- CircRNA sequencing data have been deposited at GEO and are publicly available as of the date of publication. Accession numbers are listed in the key resources table.
- This article does not report original code.
- Any additional information required to reanalyze the data reported in this paper is available from the lead contact upon request.

ACKNOWLEDGMENTS

We thank Alan Jiang and Xinsheng Xie for their support in the use of laboratory equipment. This study was supported by the National Natural Science Foundation of China (No: 82103339; 82103616).

AUTHOR CONTRIBUTIONS

XKY, YF, and TJ designed the experiment. XKY, WGX, and QWH performed the experiments. YCL and WSJ collected and analyzed the data. XKY and LYY prepared all the figures and tables. XKY wrote the original draft. All the authors have read and approved the final article.

DECLARATION OF INTERESTS

The authors declare no competing interests.

STAR★METHODS

Detailed methods are provided in the online version of this paper and include the following:

SUPPLEMENTAL INFORMATION

Supplemental information can be found online at https://doi.org/10.1016/j.isci.2024.110832.

Received: January 20, 2024
Revised: July 14, 2024
Accepted: August 23, 2024
Published: August 27, 2024

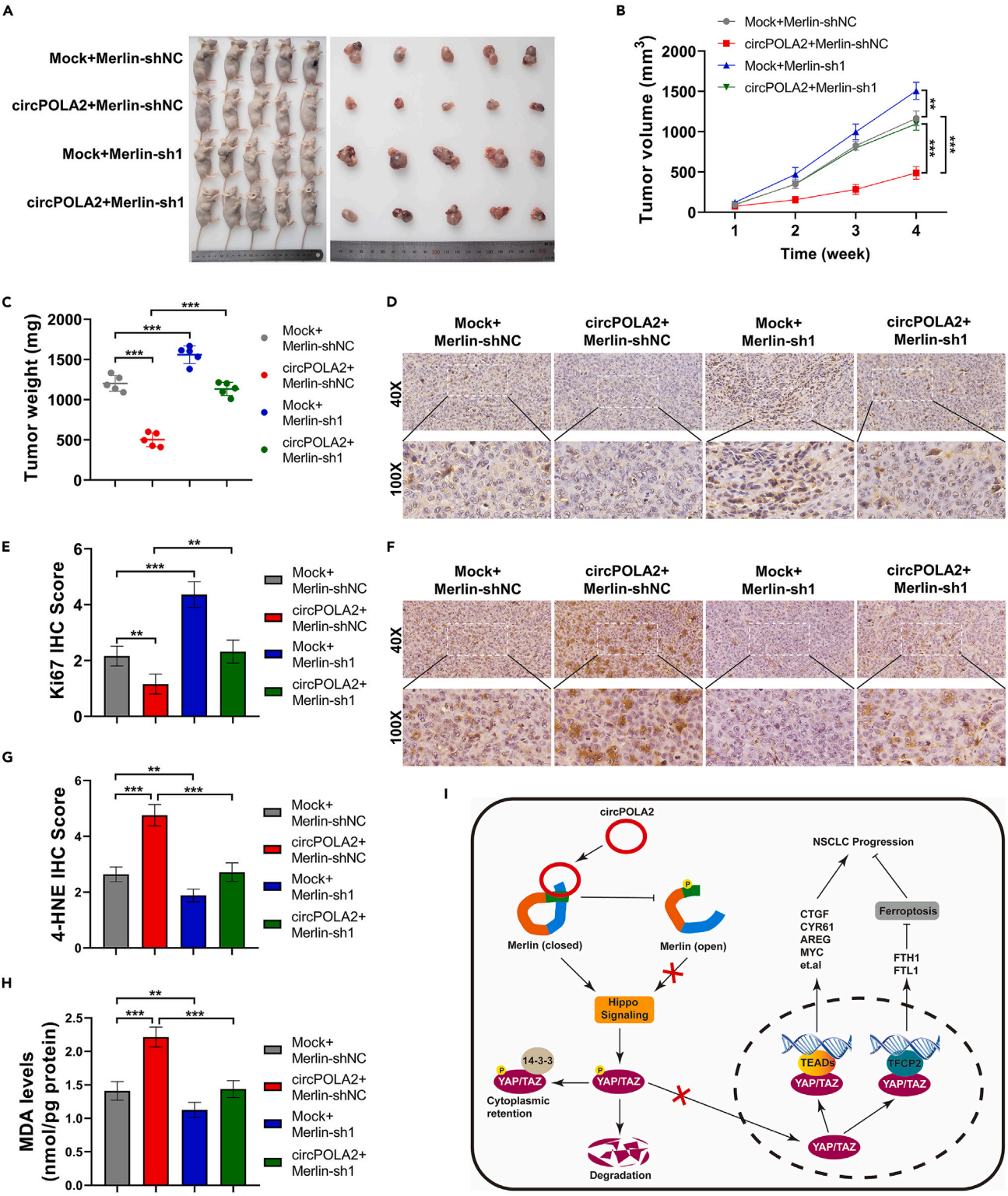

Figure 7. CircPOLA2 sensitized NSCLC cells to ferroptosis and inhibited tumorigenesis via Merlin *in vivo*

The xenograft model was established by injecting PC9 cells stably overexpressing circPOLA2 with or without Merlin-shRNAs into the flanks of BALB/c nude mice.

(A) Gross tumor appearance *in vivo* and *ex vivo*.

(B) Growth curves were plotted from tumor sizes measured weekly.

Figure 7. *Continued*

(C) Tumor weight was measured at the endpoint.

(D and E) Representative pictures of Ki-67 stained by IHC (D) and statistical analysis of the staining intensity score (E).

(F and G) Representative pictures of 4-HNE stained by IHC (F) and statistical analysis of the staining intensity score (G).

(H) MDA levels in tumor lysates were measured by colorimetry, and the results were expressed as μmol per mg protein.

(I) Schematic illustrating the role of circPOLA2 in NSCLC. Data are presented as the mean ± SD (n = 5 per group). *$p < 0.05$, **$p < 0.01$, ***$p < 0.001$.

See also Figure S5.

REFERENCES

1. Sung, H., Ferlay, J., Siegel, R.L., Laversanne, M., Soerjomataram, I., Jemal, A., and Bray, F. (2021). Global Cancer Statistics 2020: GLOBOCAN Estimates of Incidence and Mortality Worldwide for 36 Cancers in 185 Countries. CA. Cancer J. Clin. *71*, 209–249. https://doi.org/10.3322/caac.21660.
2. Chen, P., Liu, Y., Wen, Y., and Zhou, C. (2022). Non-small cell lung cancer in China. Cancer Commun. *42*, 937–970. https://doi.org/10.1002/cac2.12359.
3. Siegel, R.L., Miller, K.D., Wagle, N.S., and Jemal, A. (2023). Cancer statistics, 2023. CA. Cancer J. Clin. *73*, 17–48. https://doi.org/10.3322/caac.21763.
4. Xiao, M.S., Ai, Y., and Wilusz, J.E. (2020). Biogenesis and Functions of Circular RNAs Come into Focus. Trends Cell Biol. *30*, 226–240. https://doi.org/10.1016/j.tcb.2019.12.004.
5. Kristensen, L.S., Jakobsen, T., Hager, H., and Kjems, J. (2022). The emerging roles of circRNAs in cancer and oncology. Nat. Rev. Clin. Oncol. *19*, 188–206. https://doi.org/10.1038/s41571-021-00585-y.
6. Li, J., Zhang, Q., Jiang, D., Shao, J., Li, W., and Wang, C. (2022). CircRNAs in lung cancer- role and clinical application. Cancer Lett. *544*, 215810. https://doi.org/10.1016/j.canlet.2022.215810.
7. Dixon, S.J., Lemberg, K.M., Lamprecht, M.R., Skouta, R., Zaitsev, E.M., Gleason, C.E., Patel, D.N., Bauer, A.J., Cantley, A.M., Yang, W.S., et al. (2012). Ferroptosis: An Iron-Dependent Form of Nonapoptotic Cell Death. Cell *149*, 1060–1072. https://doi.org/10.1016/j.cell.2012.03.042.
8. Lei, G., Zhuang, L., and Gan, B. (2022). Targeting ferroptosis as a vulnerability in cancer. Nat. Rev. Cancer *22*, 381–396. https://doi.org/10.1038/s41568-022-00459-0.
9. Lei, G., Zhuang, L., and Gan, B. (2021). mTORC1 and ferroptosis: Regulatory mechanisms and therapeutic potential. Bioessays *43*, e2100093. https://doi.org/10.1002/bies.202100093.
10. Hu, K., Li, K., Lv, J., Feng, J., Chen, J., Wu, H., Cheng, F., Jiang, W., Wang, J., Pei, H., et al. (2020). Suppression of the SLC7A11/glutathione axis causes synthetic lethality in KRAS-mutant lung adenocarcinoma. J. Clin. Invest. *130*, 1752–1766. https://doi.org/10.1172/JCI124049.
11. Lim, J.K.M., Delaidelli, A., Minaker, S.W., Zhang, H.F., Colovic, M., Yang, H., Negri, G.L., von Karstedt, S., Lockwood, W.W., Schaffer, P., et al. (2019). Cystine/glutamate antiporter xCT (SLC7A11) facilitates oncogenic RAS transformation by preserving intracellular redox balance. Proc. Natl. Acad. Sci. USA *116*, 9433–9442. https://doi.org/10.1073/pnas.1821323116.
12. Liu, Y., and Gu, W. (2022). p53 in ferroptosis regulation: the new weapon for the old guardian. Cell Death Differ. *29*, 895–910. https://doi.org/10.1038/s41418-022-00943-y.
13. Zhang, Y., Shi, J., Liu, X., Feng, L., Gong, Z., Koppula, P., Sirohi, K., Li, X., Wei, Y., Lee, H., et al. (2018). BAP1 links metabolic regulation of ferroptosis to tumour suppression. Nat. Cell Biol. *20*, 1181–1192. https://doi.org/10.1038/s41556-018-0178-0.
14. Yao, W., Wang, J., Meng, F., Zhu, Z., Jia, X., Xu, L., Zhang, Q., and Wei, L. (2021). Circular RNA CircPVT1 Inhibits 5-Fluorouracil Chemosensitivity by Regulating Ferroptosis Through MiR-30a-5p/FZD3 Axis in Esophageal Cancer Cells. Front. Oncol. *11*, 780938. https://doi.org/10.3389/fonc.2021.780938.
15. Bazhabayi, M., Qiu, X., Li, X., Yang, A., Wen, W., Zhang, X., Xiao, X., He, R., and Liu, P. (2021). CircGFRA1 facilitates the malignant progression of HER-2-positive breast cancer via acting as a sponge of miR-1228 and enhancing AIFM2 expression. J. Cell Mol. Med. *25*, 10248–10256. https://doi.org/10.1111/jcmm.16963.
16. Wang, H.H., Ma, J.N., and Zhan, X.R. (2021). Circular RNA Circ_0067934 Attenuates Ferroptosis of Thyroid Cancer Cells by miR-545-3p/SLC7A11 Signaling. Front. Endocrinol. *12*, 670031. https://doi.org/10.3389/fendo.2021.670031.
17. Chen, W., Fu, J., Chen, Y., Li, Y., Ning, L., Huang, D., Yan, S., and Zhang, Q. (2021). Circular RNA circKIF4A facilitates the malignant progression and suppresses ferroptosis by sponging miR-1231 and upregulating GPX4 in papillary thyroid cancer. Aging (Albany, NY.) *13*, 16500–16512. https://doi.org/10.18632/aging.203172.
18. Shanshan, W., Hongying, M., Jingjing, F., Yiming, Y., Yu, R., and Rui, Y. (2021). CircDTL Functions as an Oncogene and Regulates Both Apoptosis and Ferroptosis in Non-small Cell Lung Cancer Cells. Front. Genet. *12*, 743505. https://doi.org/10.3389/fgene.2021.743505.
19. Zuo, Y.B., Zhang, Y.F., Zhang, R., Tian, J.W., Lv, X.B., Li, R., Li, S.P., Cheng, M.D., Shan, J., Zhao, Z., and Xin, H. (2022). Ferroptosis in Cancer Progression: Role of Noncoding RNAs. Int. J. Biol. Sci. *18*, 1829–1843. https://doi.org/10.7150/ijbs.66917.
20. Fu, M., Hu, Y., Lan, T., Guan, K.L., Luo, T., and Luo, M. (2022). The Hippo signalling pathway and its implications in human health and diseases. Signal Transduct. Targeted Ther. *7*, 376. https://doi.org/10.1038/s41392-022-01191-9.
21. Mui, C.W., Chan, W.N., Chen, B., Cheung, A.H.K., Yu, J., Lo, K.W., Ke, H., Kang, W., and To, K.F. (2023). Targeting YAP1/TAZ in nonsmall-cell lung carcinoma: From molecular mechanisms to precision medicine. Int. J. Cancer *152*, 558–571. https://doi.org/10.1002/ijc.34249.
22. Yang, W.H., Ding, C.K.C., Sun, T., Rupprecht, G., Lin, C.C., Hsu, D., and Chi, J.T. (2019). The Hippo Pathway Effector TAZ Regulates Ferroptosis in Renal Cell Carcinoma. Cell Rep. *28*, 2501–2508.e4. https://doi.org/10.1016/j.celrep.2019.07.107.
23. Yang, W.H., Huang, Z., Wu, J., Ding, C.K.C., Murphy, S.K., and Chi, J.T. (2020). A TAZ–ANGPTL4–NOX2 Axis Regulates Ferroptotic Cell Death and Chemoresistance in Epithelial Ovarian Cancer. Mol. Cancer Res. *18*, 79–90. https://doi.org/10.1158/1541-7786.MCR-19-0691.
24. Wu, J., Minikes, A.M., Gao, M., Bian, H., Li, Y., Stockwell, B.R., Chen, Z.N., and Jiang, X. (2019). Intercellular interaction dictates cancer cell ferroptosis via NF2-YAP signalling. Nature *572*, 402–406. https://doi.org/10.1038/s41586-019-1426-6.
25. Gao, R., Kalathur, R.K.R., Coto-Llerena, M., Ercan, C., Buechel, D., Shuang, S., Piscuoglio, S., Dill, M.T., Camargo, F.D., Christofori, G., and Tang, F. (2021). YAP/TAZ and ATF4 drive resistance to Sorafenib in hepatocellular carcinoma by preventing ferroptosis. EMBO Mol. Med. *13*, e14351. https://doi.org/10.15252/emmm.202114351.
26. Zhang, X., Yu, K., Ma, L., Qian, Z., Tian, X., Miao, Y., Niu, Y., Xu, X., Guo, S., Yang, Y., et al. (2021). Endogenous glutamate determines ferroptosis sensitivity via ADCY10-dependent YAP suppression in lung adenocarcinoma. Theranostics *11*, 5650–5674. https://doi.org/10.7150/thno.55482.
27. Wang, Y., Qiu, S., Wang, H., Cui, J., Tian, X., Miao, Y., Zhang, C., Cao, L., Ma, L., Xu, X., et al. (2021). Transcriptional Repression of Ferritin Light Chain Increases Ferroptosis Sensitivity in Lung Adenocarcinoma. Front. Cell Dev. Biol. *9*, 719187. https://doi.org/10.3389/fcell.2021.719187.
28. Glažar, P., Papavasileiou, P., and Rajewsky, N. (2014). circBase: a database for circular RNAs. RNA *20*, 1666–1670. https://doi.org/10.1261/rna.043687.113.
29. Wu, S., Zhu, C., Tang, D., Dou, Q.P., Shen, J., and Chen, X. (2021). The role of ferroptosis in lung cancer. Biomark. Res. *9*, 82. https://doi.org/10.1186/s40364-021-00338-0.
30. Zhou, N., Yuan, X., Du, Q., Zhang, Z., Shi, X., Bao, J., Ning, Y., and Peng, L. (2023). FerrDb V2: update of the manually curated database of ferroptosis regulators and ferroptosis-disease associations. Nucleic Acids Res. *51*, D571–D582. https://doi.org/10.1093/nar/gkac935.
31. Yin, F., Yu, J., Zheng, Y., Chen, Q., Zhang, N., and Pan, D. (2013). Spatial Organization of Hippo Signaling at the Plasma Membrane Mediated by the Tumor Suppressor Merlin/NF2. Cell *154*, 1342–1355. https://doi.org/10.1016/j.cell.2013.08.025.
32. Su, T., Ludwig, M.Z., Xu, J., and Fehon, R.G. (2017). Kibra and Merlin Activate the Hippo Pathway Spatially Distinct from and Independent of Expanded. Dev. Cell *40*, 478–490.e3. https://doi.org/10.1016/j.devcel.2017.02.004.
33. Li, W., Cooper, J., Karajannis, M.A., and Giancotti, F.G. (2012). Merlin: a tumour suppressor with functions at the cell cortex

and in the nucleus. EMBO Rep. *13*, 204–215. https://doi.org/10.1038/embor.2012.11.

34. Surace, E.I., Haipek, C.A., and Gutmann, D.H. (2004). Effect of merlin phosphorylation on neurofibromatosis 2 (NF2) gene function. Oncogene *23*, 580–587. https://doi.org/10.1038/sj.onc.1207142.
35. Fan, F., He, Z., Kong, L.L., Chen, Q., Yuan, Q., Zhang, S., Ye, J., Liu, H., Sun, X., Geng, J., et al. (2016). Pharmacological targeting of kinases MST1 and MST2 augments tissue repair and regeneration. Sci. Transl. Med. *8*, 352ra108. https://doi.org/10.1126/scitranslmed.aaf2304.
36. Zhang, X., Hou, L., Guo, Z., Wang, G., Xu, J., Zheng, Z., Sun, K., and Guo, F. (2023). Lipid peroxidation in osteoarthritis: focusing on 4-hydroxynonenal, malondialdehyde, and ferroptosis. Cell Death Discov. *9*, 320. https://doi.org/10.1038/s41420-023-01613-9.
37. Guo, J.U., Agarwal, V., Guo, H., and Bartel, D.P. (2014). Expanded identification and characterization of mammalian circular RNAs. Genome Biol. *15*, 409. https://doi.org/10.1186/s13059-014-0409-z.
38. Enuka, Y., Lauriola, M., Feldman, M.E., Sas-Chen, A., Ulitsky, I., and Yarden, Y. (2016). Circular RNAs are long-lived and display only minimal early alterations in response to a growth factor. Nucleic Acids Res. *44*, 1370–1383. https://doi.org/10.1093/nar/gkv1367.
39. Bosson, A.D., Zamudio, J.R., and Sharp, P.A. (2014). Endogenous miRNA and Target Concentrations Determine Susceptibility to Potential ceRNA Competition. Mol. Cell *56*, 347–359. https://doi.org/10.1016/j.molcel.2014.09.018.
40. Zhou, W.Y., Cai, Z.R., Liu, J., Wang, D.S., Ju, H.Q., and Xu, R.H. (2020). Circular RNA: metabolism, functions and interactions with proteins. Mol. Cancer *19*, 172. https://doi.org/10.1186/s12943-020-01286-3.
41. Yang, F., Liu, Y., Xiao, J., Li, B., Chen, Y., Hu, A., Zeng, J., Liu, Z., and Liu, H. (2023). Circ-CTNNB1 drives aerobic glycolysis and osteosarcoma progression via m6A modification through interacting with RBM15. Cell Prolif. *56*, e13344. https://doi.org/10.1111/cpr.13344.
42. Xie, F., Huang, C., Liu, F., Zhang, H., Xiao, X., Sun, J., Zhang, X., and Jiang, G. (2021). CircPTPRA blocks the recognition of RNA N(6)-methyladenosine through interacting with IGF2BP1 to suppress bladder cancer progression. Mol. Cancer *20*, 68. https://doi.org/10.1186/s12943-021-01359-x.
43. Li, B., Zhu, L., Lu, C., Wang, C., Wang, H., Jin, H., Ma, X., Cheng, Z., Yu, C., Wang, S., et al. (2021). circNDUFB2 inhibits non-small cell lung cancer progression via destabilizing IGF2BPs and activating anti-tumor immunity. Nat. Commun. *12*, 295. https://doi.org/10.1038/s41467-020-20527-z.
44. Mota, M., and Shevde, L.A. (2020). Merlin regulates signaling events at the nexus of development and cancer. Cell Commun. Signal. *18*, 63. https://doi.org/10.1186/s12964-020-00544-7.
45. Xing, N., Du, Q., Guo, S., Xiang, G., Zhang, Y., Meng, X., Xiang, L., and Wang, S. (2023). Ferroptosis in lung cancer: a novel pathway regulating cell death and a promising target for drug therapy. Cell Death Discov. *9*, 110. https://doi.org/10.1038/s41420-023-01407-z.
46. Magesh, S., and Cai, D. (2022). Roles of YAP/TAZ in ferroptosis. Trends Cell Biol. *32*, 729–732. https://doi.org/10.1016/j.tcb.2022.05.005.
47. Li, D., Song, H., Mei, H., Fang, E., Wang, X., Yang, F., Li, H., Chen, Y., Huang, K., Zheng, L., and Tong, Q. (2018). Armadillo repeat containing 12 promotes neuroblastoma progression through interaction with retinoblastoma binding protein 4. Nat. Commun. *9*, 2829. https://doi.org/10.1038/s41467-018-05286-2.
48. Guo, R., Ma, L., Bai, X., Miao, L., Li, Z., and Yang, J. (2021). A Scoring Method for Immunohistochemical Staining on Ki67. Appl. Immunohistochem. Mol. Morphol. *29*, e20–e28. https://doi.org/10.1097/PAI.0000000000000853.

STAR★METHODS

KEY RESOURCES TABLE

REAGENT or RESOURCE	SOURCE	IDENTIFIER
Antibodies		
Rabbit monoclonal anti-Merlin	Cell Signaling Technology	Cat#12888; RRID: AB_2650551
Rabbit monoclonal anti-Phospho-Merlin (Ser518)	Cell Signaling Technology	Cat#13281; RRID: AB_2650552
Rabbit monoclonal anti-YAP	Cell Signaling Technology	Cat#14074; RRID: AB_2650491
Rabbit polyclonal anti-Phospho-YAP (Ser127)	Cell Signaling Technology	Cat#4911; RRID: AB_2218913
Rabbit monoclonal anti-LATS1	Cell Signaling Technology	Cat#3477; RRID: AB_2133513
Rabbit monoclonal anti-Phospho-LATS1 (Thr1079)	Cell Signaling Technology	Cat#8654; RRID: AB_10971635
Rabbit monoclonal anti-Flag	Cell Signaling Technology	Cat#14793; RRID: AB_2572291
Mouse monoclonal anti-Ki-67	Cell Signaling Technology	Cat#9449; RRID: AB_2797703
Mouse monoclonal anti-4 Hydroxynonenal	Abcam	Cat#ab48506; RRID: AB_867452
Rabbit polyclonal anti-β-actin	Proteintech	Cat#20536-1-AP; RRID: AB_10700003
HRP-conjugated Goat Anti-Rabbit IgG(H+L)	Proteintech	Cat#SA00001-2; RRID: AB_2722564
FITC-labeled goat anti-rabbit IgG	Proteintech	Cat#SA00003-2; RRID: AB_2890897
Rabbit IgG control Polyclonal antibody	Proteintech	Cat#30000-0-AP; RRID: AB_2819035
Bacterial and virus strains		
DH5α Fast Chemically Competent Cell	Yeasen Biotechnology (Shanghai) Co., Ltd.	Cat#11803ES80
pLCDH-ciR	Geenseed Biotech	Cat#GS0103
pCDH-CMV-EF1-Neo	MiaoLing Biology	Cat#P13674
pLKO.1-Puro	MiaoLing Biology	Cat#P0258
Biological samples		
Human NSCLC tissues and adjacent normal tissues	The First Affiliated Hospital of Nanchang University	N/A
Chemicals, peptides, and recombinant proteins		
Lipofectamine 3000	Invitrogen	Cat#L3000075
TRIzol reagent	Invitrogen	Cat#15596026
BODIPY™ 581/591 C11	Invitrogen	Cat#D3861
Streptavidin magnetic beads	Invitrogen	Cat#65001
RNase inhibitor	Takara	Cat#2313A
Protease inhibitor cocktail	MCE	Cat#HY-K0010
Phosphatase Inhibitor Cocktail II	MCE	Cat#HY-K0022
Erastin	MCE	Cat#HY-15763
Ferrostatin-1	MCE	Cat#HY-100579
Deferoxamine mesylate (DFO)	MCE	Cat#HY-B0988
Z-VAD-FMK	MCE	Cat#HY-16658B
3-methylademine (3-MA)	MCE	Cat#HY-19312
Ncerostatin-1 (Nec-1)	MCE	Cat#HY-15760
Actinomycin D	MCE	Cat#HY-17559
Ultra GelRed	Vazyme	Cat#GR501-01
RNase R	Beyotime	Cat#R7092M

(*Continued on next page*)

Continued

REAGENT or RESOURCE	SOURCE	IDENTIFIER
XMU-MP-1	Selleck	Cat#S8334
Critical commercial assays		
Fast Silver Stain Kit	Beyotime	Cat#P0017S
Lipid Peroxidation MDA Assay Kit	Beyotime	Cat#S0131M
Magna RIP Kit	Millipore	Cat#17-700
EZ-press RNA Purification Kit	EZBioscience	Cat#B0004D
Universal Genomic DNA Kit	CoWin Biotech	Cat#CW2298S
CellTiter-Glo® Luminescent Cell Viability Assay	Promega	Cat#G7572
Cell Counting Kit-8	Dojindo	Cat#CK04
Chemiluminescene Kit	Thermo	Cat#32109
Edu Apollo *In Vitro* Kit	Ribobio	Cat#C10310-2
Annexin V-APC/PI apoptosis detection kit	Bestbio	Cat#BB-41033
PARIS™ Kit	Life Technologies	Cat#AM1921
PrimeScript RT reagent Kit	Takara	Cat#RR037A
PrimeSTAR Max Premix	Takara	Cat#R045A
SYBR qPCR Master Mix kit	Vazyme	Cat#Q712
2-step plus Poly-HRP Anti Rabbit/Mouse IgG Detection Syste (with DAB Solution)	Elabscience	Cat#E-IR-R213
Deposited data		
CircRNA sequencing data	This paper	GEO: GSE254362
circPOLA2 location on chromosome	UCSC Genome Browser	https://genome.ucsc.edu/
Expression profiles of circRNAs in NSCLC	GEO DetaSets	GSE101684; GSE112214
Annotation of circPOLA2	circBase	http://circbase.org/
Ferroptosis regulators	FerrDb	http://www.zhounan.org/ferrdb/current/
Experimental models: Cell lines		
A549	ATCC	CCL-185
PC-9	Cell Bank/Stem Cell Bank, Chinese Academy of Sciences	SCSP-5085
H1299	ATCC	CRL-5803
H1975	ATCC	CRL-9482
BBM	ATCC	CRL-9482
293T	ATCC	CRL-3216
Experimental models: Organisms/strains		
Female BALB/c nude mice	Beijing Vital River Laboratory Animal Technology Co., Ltd.	N/A
Oligonucleotides		
Primers used for RT-PCR and RT-qPCR, see Table S1	Beijing Tsingke Biotech Co., Ltd.	N/A
Oligonucleotides and primers used for RNA pull-down, FISH and vector cloning, see Table S2	Beijing Tsingke Biotech Co., Ltd.	N/A
Recombinant DNA		
pCMV-3Tag-1A (NF2-FERM)	Agilent	N/A
pCMV-3Tag-1A (NF2-FULL)	Agilent	N/A

(*Continued on next page*)

Continued

REAGENT or RESOURCE	SOURCE	IDENTIFIER
pCMV-3Tag-1A (NF2-ΔC)	Agilent	N/A
pCMV-3Tag-1A (NF2-ΔFERM)	Agilent	N/A
Software and algorithms		
Image-Pro Plus (version 6.0)	Media Cybernetics	https://mediacy.com/image-pro/
IBM SPSS Statistics (version 26.0)	IBM Corp	https://www.ibm.com/support/pages/downloading-ibm-spss-statistics-26
FlwoJo (version 10.8.1)	BD Life Sciences	https://www.flowjo.com/solutions/flowjo/downloads
GraphPad Prism (version 8.0.1)	GraphPad	https://www.graphpad-prism.cn/

EXPERIMENTAL MODEL AND STUDY PARTICIPANT DETAILS

Patients and tissue samples

NSCLC tissues and adjacent normal tissues were obtained from 51 patients (Table 1) who underwent surgical resection at the First Affiliated Hospital of Nanchang University. The inclusion criteria were age 18-80 years, primary lung cancer at first treatment, no preoperative treatment, and postoperative pathologically confirmed NSCLC. The study was approved by the Ethics Committee of the First Affiliated Hospital of Nanchang University and carried out in accordance with the Helsinki principles. Written informed consent was obtained from all patients. Fresh tissue samples were immediately frozen in liquid nitrogen and stored at -80°C until use.

Cell lines and cell culture

The human NSCLC cell lines A549, H1975, and H1299 and the human normal bronchial epithelial cell line BBM were acquired from the American Type Culture Collection (ATCC, USA). The human NSCLC cell line PC9 was purchased form Cell Bank/Stem Cell Bank, Chinese Academy of Sciences. Human embryonic kidney cells (HEK-293T) were maintained in our laboratory. PC9, H1975, and H1299 cells were cultured in RPMI 1640 (Gibco, China) supplemented with 10% FBS and 1% penicillin-streptomycin. A549 and HEK-293T cells were cultured in DMEM (Gibco, China) supplemented with 10% FBS and 1% penicillin-streptomycin. All cells were cultured in a humidified incubator at 37°C with 5% CO2.

Tumor xenograft model

Female BALB/c nude mice (3-4 weeks old) were purchased from Beijing Vital River Laboratory Animal Technology Co., Ltd. (Beijing, China). A subcutaneous tumor bearing nude mouse model was established by injecting 5×10^6 PC9 cells into the flanks of BALB/c nude mice. Prior to injection, PC9 cells were stably transfected with a circPOLA2 overexpression construct, Merlin knockdown construct, or empty vector. Tumor size was measured weekly, and the tumor volume was calculated as follows: $0.52\times length\times width^2$. All mice were euthanized after 4 weeks, and xenografts were weighed and collected. All animal experiments were performed in accordance with the guidelines of the National Institutes of Health, and were approved by the Animal Use and Care Committee of NanChang University.

METHOD DETAILS

RNA sequencing and data analysis

CircRNA library preparation and high-throughput sequencing and data analysis were performed by SeqHealth Technology Co., Ltd. (Wuhan, China). Briefly, total RNA was extracted from 4 paired NSCLC tissues and adjacent normal lung tissues using TRIzol reagent (Invitrogen, Cat#15596026, USA). The RNA samples were then sequentially treated with DNase I, rRNA Depletion Kit, and RNase R to remove DNA, ribosomal RNA, and linear RNA respectively. Finally, the library products corresponding to 200-500 bp were enriched, quantified and sequenced on a DNBSEQ-T7 sequencer (MGI Tech Co., Ltd. China) with the PE150 model. Differentially expressed circRNAs between groups were identified using the edgeR package (version 3.12.1). $P \leq 0.05$ was used as the cutoff to assess the statistical significance of circRNA expression differences. All differentially expressed circRNAs are listed in Table S4.

Reverse transcription PCR (RT-PCR) and real-time quantitative PCR (RT-qPCR)

Total RNA was extracted with the EZ-press RNA Purification Kit (EZBioscience, B0004D, USA), nuclear and cytoplasmic RNA was fractionated by the PARIS™ Kit (Life Technologies, AM1921, USA) according to the manufacturer's instructions. Reverse transcription was performed with a commercial kit (Takara, RR037A, Japan) using oligo(dT) or random 6-mer primers. Genomic DNA was extracted using the Universal Genomic DNA Kit (CoWin Biotech, CW2298S, China). RT-PCR was performed using the PrimeSTAR Max Premix (Takara, R045A, Japan), and the products were visualized via electrophoresis on 1.5% agarose gel added with Ultra GelRed (Vazyme, GR501-01, China) stain. RT-qPCR was performed using the SYBR qPCR Master Mix kit (Vazyme, Q712, China), and the gene expression was calculated using the $2^{-\Delta\Delta CT}$ method. All the PCR primer sequences are presented in Table S1.

Fluorescence *in situ* hybridization (FISH) and immunofluorescence (IF)

A Cy3-labeled antisense probe (Table S2) for circPOLA2 was synthesized by Beijing Tsingke Biotech Co., Ltd. (Beijing, China). Lung cancer cells were cultured on coverslips, incubated with primary antibody specific for Merlin (Cell Signaling Technology, #12888, USA, 1:200 dilution) at 4°C overnight, treated with FITC-labeled goat anti-rabbit IgG (Proteintech, SA00003-2, China, 1:1000 dilution) at room temperature for 2 h, and then incubated with the FISH probe at 50°C for 4 h. Finally, the cell nuclei were stained with DAPI (4′6-diamidino-2-phenyhlindole). Images were captured using a Leica Stellaris 5 confocal microscope (Germany).

Plasmids, lentivirus, and cell transfection

For circPOLA2 overexpression, full-length circPOLA2 was amplified by PCR from POLA2 cDNA using specific primers. The purified linear circPOLA2 fragment was subcloned and inserted into a modified pLCDH-ciR vector (Geenseed Biotech, China). For the expression of flag-tagged wild-type and truncated merlin, full-length and truncated CDSs were amplified from a plasmid (pOTB7-NF2-2) containing the CDS of merlin (MiaoLing Biology, China) and then subcloned and inserted into the vector pCMV-3Tag-1A (Agilent, USA). For the overexpression of mutant merlin (S518A), a pair of ligament primers containing the mutated site was used for PCR-mediated site-directed mutagenesis, and then the mutant merlin CDS was inserted into the vector pCDH-CMV-EF1-Neo (MiaoLing Biology, China). For knockdown constructs, shRNAs targeting circPOLA2 and merlin were synthesized by Beijing Tsingke Biotech Co. (Beijing, China) and then subcloned and inserted into the pLKO.1-Puro vector (MiaoLing Biology, China). All plasmids were transfected using Lipofectamine 3000 reagent (Invitrogen, L3000075, USA). Two auxiliary vectors, pMD2.G and psPAX2, were used for lentiviral packaging in HEK 293T cells. Stable cell lines were obtained via neomycin or puromycin (Invitrogen) selection for 2-3 weeks. All primers and oligonucleotides used for vector cloning are listed in Table S2.

RNA pull-down and mass spectrometry

Biotin-labeled sense (as a negative control) and antisense probes (Table S2) for the circPOLA2 back-splicing site were synthesized by Beijing Tsingke Biotech Co. (Beijing, China). RNA pull-down assay was performed as follows: Briefly, A549 cell lysates were first prepared using IP lysis buffer (Thermo, 87787, USA) supplemented with protease inhibitor cocktail (MCE, HY-K0010, USA) and RNase inhibitor (Takara, 2313A, Japan); second, biotinylated probes were bound to streptavidin magnetic beads (Invitrogen, 65001, USA); third, cell lysates were added to the probe-conjugated streptavidin magnetic beads and incubated overnight at 4°C; finally, the RNA-binding protein complexes were collected and washed for further testing. A small fraction of the RNA pull-down products was separated by SDS-PAGE, followed by silver staining using a Fast Silver Stain Kit (Beyotime, P0017S, China). The remaining fraction was analyzed by mass spectrometry (MS) by SpecAlly Life Technology Co., Ltd (Wuhan, China). All significantly enriched proteins are listed in Table S3.

RNA immunoprecipitation (RIP) assay

The RIP assay was performed using the Magna RIP Kit (Millipore, 17-700, USA) according to the manufacturer's protocol. Antibodies specific for Merlin (CST, #12888, USA) and Flag-tag (CST, #14793, USA) and negative control rabbit IgG (Proteintech, 30000-0-AP, China) were used. Input and coimmunoprecipitated RNAs were extracted using the EZ-press RNA Purification Kit (EZBioscience, B0004D, USA) and subjected to RT-PCR or RT-qPCR.

Lipid peroxidation measurement

Cells were seeded in 6-well plates and cultured overnight. The following day, the cells were treated with reagents for the indicated times. The cells were then incubated with BODIPY™ 581/591 C11 (Invitrogen, D3861, USA) for 30 minutes before harvesting. Lipid peroxidation was measured using a flow cytometer (NovoCyte D3000, Agilent, USA) with a 488 nm laser on a B530 detector. The flow cytometry results were analyzed using FlowJo™ v10.8.1 Software (BD Life Sciences), and the mean fluorescence intensity was used for statistical analysis. Cells were cultured on coverslips for fluorescence imaging. After staining with BODIPY™ 581/591 C11, nuclei were stained with DAPI. Images were taken with a Leica Stellaris 5 confocal microscope (Germany).

Malondialdehyde (MDA) assay

Intracellular MDA levels were measured to determine the level of lipid peroxidation. Cells were seeded in 6-well plates and incubated with the indicated treatments. MDA levels were tested using the Lipid Peroxidation MDA Assay Kit (Beyotime, S0131M, China) according to the manufacturer's instructions. The results are presented as μmol per mg protein.

Transmission electron microscopy (TEM) imaging

To observe the morphological changes in mitochondria, PC9 cells stably transfected with circPOLA2 overexpression or empty plasmid were seeded into 10 cm dishes. After 12 hours, the cells were treated with erastin (10 μmol/L) or DMSO for 20 hours. The cells were fixed with 2.5% glutaraldehyde in 0.1 M PBS for 2 hours at 4°C. The cells were then scraped, collected and postfixed in 1% OsO4 for 2 hours at 4°C. The samples were then dehydrated through graded ethanol solutions and subsequently embedded in epoxy resin. Ultrathin sections were prepared, stained with 2% uranyl acetate and examined using an HT7800 transmission electron microscope (HITACHI, Japan).

Cell migration and invasion assays

Transwell assays were used to evaluate the migration and invasion ability of NSCLC cells *in vitro*. After 8 hours of serum starvation, A549 or PC9 cells were collected and adjusted to a concentration of 1×10^5 in 200 μl of serum-free medium, and plated into the upper chamber (Costar; Corning, Inc; pore size: 3 μm; Cat. No. 3495), which were coated with (for invasion assay) or without (for migration assay) 2% Matrigel (Corning, USA). Chambers were incubated in a 24-well plate containing 750 μl medium supplemented with 20% FBS as a nutrient attractant. After culturing for 12 h (for migration assay) or 24 h (for invasion assay), the chambers were collected, fixed with 4% polyformaldehyde, and stained with 0.5% crystal violet. Cells on the upper chamber membrane were wiped off with a cotton swab. The migrated or invaded cells were photographed in five randomly selected fields under an orthotopic microscope (ZEISS Axio Lab.A1, Germany). The number of cells was calculated using Image-Pro Plus version 6.0 (Media Cybernetics, Silver Spring, MD, USA).

Cell proliferation assay

For the Cell Counting Kit-8 (CCK-8, Dojindo, Japan) assay, cells were seeded in 96-well plates (1000 cells per well) and cell proliferation rates were monitored for the following 4 days. Briefly, 10 μl of CCK-8 reagent and 100 μl of complete medium were mixed and added to each well. After incubation for 2 h at 37°C away from light, absorbance was measured at 450 nm using a microplate reader. Each group set up three technical replicates, and the assay was independently repeated three times. For the Edu (5-Ethynyl-2′-deoxyuridine; Ribobio, China) assay, cells were cultured in a 24-well plate for 24 h, followed by incubation with a 50mM Edu solution for 2 h, and then fixed in 4% paraformaldehyde, followed by permeabilization with 0.3% Triton for 10 min. then sequentially stained with Apollo® 643 and Hoechst 33342. The EdU-positive cells were imaged with Leica Stellaris 5 Confocal Microscope (Germany), and counted using Image-Pro Plus version 6.0.

Cell viability and death assay

For the cell viability assay, cells were seeded in a lightproof 96-well plates (3000 cells per well) and incubated with the indicated treatments for the appropriate time. Cell viability was tested using the CellTiter-Glo Viability Assay (Promega, G7572) according to the manufacturer's instructions. Chemiluminescence signals were detected using a bioluminescence plate reader (Berthold Centro LB 960), and the results were presented as relative ATP levels. Dead cells were double stained with Annexin V-APC and PI (Bestbio, BB-41033, China) and measured by flowcytometry with NovoCyte D3000 (Agilent, USA). The flow cytometry results were analyzed using FlowJo™ v10.8.1 Software (BD Life Sciences).

Western blotting

Proteins were extracted by the RIPA lysis buffer (Thermo, USA) and separated through SDS-PAGE followed by transfer to PVDF membranes (Millipore, USA). Proteins on the PVDF membranes were incubated with primary antibodies for Flag-tag (CST, #14793, USA), Merlin (CST, #12888, USA), p-Merlin (s518) (CST, #13281, USA), Lats1(CST, #3477, USA), p-Lats1(Thr1079) (CST, #8654, USA), YAP (CST, #14074, USA), p-YAP(Ser127) (CST, #4911, USA), and β-actin (Proteintech, 20536-1-AP, China) at 4°C overnight. They were then incubated with HRP-conjugated secondary antibody (Proteintech, SA00001-2, China) for 1 hour at room temperature. Finally, the blots were visualized with an enhanced chemiluminescene kit (Thermo, 32109, USA) on the Bio-Rad chemiluminescence system.

Immunohistochemistry (IHC)

Tissues were fixed with 4% paraformaldehyde and embedded in paraffin, then sliced into 5 μm slices. IHC was carried out with a commercial kit (Elabscience, E-IR-R213, China) according to the manufacture's instruction. Primary antibodies for Ki-67(1:800, CST, #9449, USA) and 4 hydroxynonenal (4-HNE) (1:200, abcam, ab48506, USA) were used. Images were captured by a ZEISS Axio Lab.A1 microscope (Germany) and blindly evaluated by two pathologists. The staining intensity was scored on a scale of 0 to 3 (0, negative; 1, weakly positive; 2, moderately positive; 3, strongly positive) and the percentage of positive cells was scored on a scale of 0 to 4 (0, negative; 1, positive in 1%-25%; 2, positive in 26%-50%; 3, positive in 51%-75%; 4, positive in 76%-100%).[47,48] The products of staining intensity multiplied by the percentage of positive cells were used for statistical analysis.

Reagents and treatments

To study the stability of RNAs, total RNA (2 μg) was incubated with 4 U/μg RNase R (Beyotime, R7092M, China) for 30 min at 37°C. A549 cells were seeded in six-well plate and treated with 2 μg/ml actinomycin D (MCE, HY-17559, USA) when the cells reached 60-70% confluence, then harvested at the indicated time points. To study cell ferroptosis, the ferroptosis inducer erastin (MCE, HY-15763, USA) was used at the indicated concentration; the ferroptosis inhibitors ferrostatin-1 (MCE, HY-100579, USA) and DFO (MCE, HY-B0988, USA) were used at 1μmol/L and 50μmol/L respectively; apoptosis inhibitor Z-VAD-FMK (MCE, HY-16658B, USA) at 10μmol/L, autophagy inhibitor 3-methylademine (3-MA) (MCE, HY-19312, USA) at 2mmol/L, and necroptosis inhibitor ncerostatin-1 (Nec-1) (MCE, HY-15760, USA) at 10μmol/L. The expression of circPOLA2 and its linear counterpart POLA2 mRNA were measured by RT-qPCR. For inhibition of the Hippo pathway, XMU-MP-1 (Selleck, S8334, USA) was added to the culture medium at a concentration of 3μM.

QUANTIFICATION AND STATISTICAL ANALYSIS

All data are expressed as the mean ± SD unless otherwise stated. For numerical variables, Student's t test and ANOVA were used for comparisons between two groups or among multiple groups respectively, and Bonferroni's correction was used for post hoc analysis after ANOVA. Clinical characteristics were analyzed using the chi-squared test and Spearman's coefficient. Statistical analyses were performed using IBM SPSS Statistics (version 26.0), and $P < 0.05$ was considered to indicate significance (*$P < 0.05$; **$P < 0.01$; ***$P < 0.001$).